Alternative splicing of *CNOT7* diversifies CCR4–NOT functions

Clément Chapat[1,*], Kamel Chettab[1], Pierre Simonet[1], Peng Wang[2], Pierre De La Grange[3], Muriel Le Romancer[1] and Laura Corbo[1]

[1]Univ. Lyon, Université Lyon 1, Inserm U1052, CNRS UMR5286, Centre Léon Bérard, Centre de Recherche en Cancérologie de Lyon, Lyon 69008, France, [2]McGill University, Department of Biochemistry, 1160 Pine Avenue West, Montreal, QC H3A 1A3, Canada and [3]GenoSplice, ICM, Pitié-Salpêtrière hospital, Paris 75013, France

ABSTRACT

The CCR4-associated factor CAF1, also called CNOT7, is a catalytic subunit of the CCR4–NOT complex, which has been implicated in all aspects of the mRNA life cycle, from mRNA synthesis in the nucleus to degradation in the cytoplasm. In human cells, alternative splicing of the C*NOT7* gene yields a second CNOT7 transcript leading to the formation of a shorter protein, CNOT7 variant 2 (CNOT7v2). Biochemical characterization indicates that CNOT7v2 interacts with CCR4–NOT subunits, although it does not bind to BTG proteins. We report that CNOT7v2 displays a distinct expression profile in human tissues, as well as a nuclear sub-cellular localization compared to CNOT7v1. Despite a conserved DEDD nuclease domain, CNOT7v2 is unable to degrade a poly(A) tail *in vitro* and preferentially associates with the protein arginine methyltransferase PRMT1 to regulate its activity. Using both *in vitro* and *in cellulo* systems, we have also demonstrated that CNOT7v2 regulates the inclusion of CD44 variable exons. Altogether, our findings suggest a preferential involvement of CNOT7v2 in nuclear processes, such as arginine methylation and alternative splicing, rather than mRNA turnover. These observations illustrate how the integration of a splicing variant inside CCR4–NOT can diversify its cell- and tissue-specific functions.

INTRODUCTION

The CCR4–NOT complex is an evolutionarily conserved multi-subunit complex which regulates several aspects of eukaryotic gene expression, including the repression and activation of mRNA synthesis, deadenylation and subsequent degradation of mRNA, and even protein degradation (for review, see (1–4)). CCR4–NOT plays a crucial role in post-transcriptional mRNA regulation in eukaryotes, from yeast to metazoans, catalyzing the removal of mRNA poly(A) tails, thereby committing mRNA to degradation. The conserved core of the complex is assembled around CNOT1, which acts as a scaffold for the assembly of three distinct modules: a deadenylase module comprising two exoribonucleases (CNOT7/CAF1a/b and CCR4a/b) surrounded by CNOT9, the NOT module containing at least CNOT2 and CNOT3, and a third distinct module composed of CNOT10 and CNOT11 that interacts with the N-terminal part of CNOT1 (5–7).

The deadenylase module consists of the yeast Ccr4 protein, or its human orthologues CNOT6 (hCCR4a) and CNOT6L (hCCR4b), which contain an exonuclease/endo nuclease/phosphatase (EEP) signature (8,9), and the yeast Caf1, or its human orthologues CNOT7 (hCAF1) and CNOT8 (hPOP2/Calif), which have RNA nuclease activities attributed to a DEDD motif (10,11). The central MIF4G domain of CNOT1 recognizes CNOT7, which in turn binds and bridges CNOT6. The CCR4–NOT complex can be recruited to mRNAs by a plethora of RNA-binding proteins and adaptors (e.g. BTG/Tob, GW182, Nanos, etc.), which mediate deadenylation and subsequent mRNA decay (1–4). Several studies have highlighted the key role of the MIF4G domain of CNOT1 as a deadenylation-independent translational repressor, by favoring the incorporation of DDX6 to the CCR4–NOT complex. Subsequently, DDX6 can recruit several silencing factors such as Pat1, Edc3, Lsm14, 4E-T and 4EHP (6,12–16). Notably, the CNOT subunits have been shown to localize to cytoplasmic P-bodies with translationally repressed mRNA and miRNAs (17,18).

The functions of CCR4–NOT are not confined to post-transcriptional regulation in the cytoplasm. The complex plays a functional role in nuclear mRNA synthesis and pro-

cessing pathways. In particular, yeast CCR4–NOT regulates transcription initiation and elongation by affecting the function of TBP/TFIID and elongating RNA polymerase II activity (19–21). Human CNOT subunits differentially influence nuclear receptor-mediated transcription, as well as the STAT1-dependent activation of interferon responsive genes (22–24). In addition, most CCR4–NOT subunits co-purify nuclear RNA processing machineries, such as splicing factors and nuclear pore complex proteins (25). Notably, human CNOT7 is a regulator of PRMT1, the predominant protein arginine methyltransferase. Both proteins interact *in vivo* and co-localize in speckles, a sub-nuclear compartment enriched in heterogeneous nuclear ribonucleoproteins (hn-RNP) and splicing factors (26). Yeast CCR4–NOT also interacts with the arginine methyltransferase, Hmt1, and two of its substrates: the hnRNPs, Nab2 and Hrp1 (27).

Despite increasing evidence that CCR4–NOT is involved in a wide variety of biological processes, relatively little is known about how the complex integrates these multiple pathways. One of the mechanisms proposed is through the modulation of its interactions with different partners and its cellular compartmentalization. For example, the subcellular localization of human CNOT7 and its interactions with distinct BTG2-containing CCR4–NOT complexes appear to be strongly dependent on cell-cycle progression (28). Another possible source of functional diversity lies in the fact that alternative splicing of the human *CNOT* genes generates a plethora of distinct isoforms with unknown functions. Notably, expression of the human *CNOT7* gene can be modified by the inclusion of an alternative 3′ terminal exon, which yields a second mRNA isoform, CNOT7v2, resulting in a protein shorter by 41-residues at its C-terminal extremity. This type of splicing event is found in >3000 human genes and corresponds to the alternative use of intronic poly(A) sites in a splicing-dependent manner (29,30).

Here, we describe the expression of CNOT7v2 in a wide variety of human tissues and breast tumors. Biochemical characterization revealed that CNOT7v2 does not display a deadenylase activity and has no affinity for the BTG proteins. Moreover, we demonstrate that CNOT7v2 associates with the CCR4–NOT subunits and is preferentially involved in the regulation of PRMT1-dependent arginine methylation.

MATERIALS AND METHODS

Cell culture

MCF7, U251 and HEK293T cells were routinely maintained in DMEM supplemented with 10% fetal bovine serum and penicillin/streptomycin in a humidified atmosphere of 5% CO_2 at 37°C. For analysis of mRNA stability, 5 μg/ml actinomycin D (Sigma) was added to the culture medium.

Normal tissues, tumor samples and total RNA extraction

Total RNA samples from various human tissues were a gift from Dr Cécile Caron (IAB, Grenoble). The breast tumor samples from women with primary breast tumors, who had not received any therapy before surgery, were from the

BB-0033-00050 'Centre de Ressources Biologiques' (Biological Resource Center) of the Center Léon Bérard (Lyon, France). The total RNA samples from human adult normal breast donors were purchased from Ambion, Agilent and Biochain. Total RNA was prepared from cell lines or tumor samples using the TRI-Reagent (Sigma), and RNA integrity was verified using the BioAnalyzer 2100 (Agilent Technologies).

Chromatography on superose 6

Cellular extract, 4 mg, from ∼5 × 10^8 MCF7 cells was prepared and fractionated on a 24 ml Superose 6 column (HR 10/30, Amersham Pharmacia Biotech) as previously described (28).

Plasmid DNA

The full-length cDNAs encompassing the coding regions of CNOT7v1 and v2, obtained by RT-PCR using total RNA from MCF7 cells, were cloned into the pSG5-Flag vector. For recombinant protein expression, the CNOT7v1 and v2 coding regions, contained in a BamHI–BglII cDNA fragment, were cloned into the pGEX-2T vector. For mammalian two-hybrid assays, CNOT7v1 and v2 cDNAs were cloned in frame with the yeast GAL4 DNA-binding domain or VP16 activation domain into the Gal4polyII and pSG-FNV vectors described in (31). The GAL4-fused BTG1 and BTG2 and the pG4-TK-Luc reporter plasmids were already described (31). To create λN-V5 expression plasmids, PCR was used to construct cDNAs encoding CNOT7v1 or v2, which were inserted as XhoI–XbaI fragments into the pCI-λN-V5 plasmid. Mutation to inactivate the active sites (D40A) was introduced by site-directed mutagenesis using the QuickChange Kit (Stratagene).

Protein extraction, immunoprecipitation, western blot and antibodies

We carried out protein extractions, immunoprecipitations (IP) and western blot as described previously (26). Extracts of total proteins from MCF7 cells were obtained as described in (32). The affinity-purified rabbit polyclonal antibody against hCNOT7 was previously described (28). Anti-CNOT1, CNOT3 and CNOT10 were purchased from Proteintech (14276-1-AP, 11135-1-AP and 15938-1-AP, respectively), and anti-CNOT2 (6955) and anti-CNOT6 (13415) from Cell Signaling. For IP and/or immunofluorescence (IF) analyses, the mouse polyclonal anti-CNOT7 (AO1) from Abnova and the mouse monoclonal anti-V5 tag from Invitrogen were used. Anti-PRMT1 (07–404) and anti-SAM68 (07–415) antibodies were purchased from Upstate Biotechnology, while the anti-GAPDH (clone 6C5) was supplied by Biodesign International. The other antibodies used recognized alpha-Tubulin (sc-23948, Santa Cruz Biotechnology), DDX6 (A300-460A, Bethyl Laboratories), CD44 (ab6124, Abcam), CD44v5 (BMS115, eBioscience), ASYM24 (EMD Millipore) and Flag (M2 Sigma).

Immunofluorescence

Cells were grown on coverslips in 12-well plates. For the anti-V5 IF assays, cells were transfected with 100 ng of pCI

vector encoding the V5-tagged CNOT7 proteins, treated as previously described (26) and visualized under a Zeiss Axioplan 2 or LSM800 confocal microscope. Intensity line scans were performed using ImageJ.

Real-Time RT-PCR

One μg of total RNA, purified using the TRI-Reagent, was reverse-transcribed using 100 ng of random primers following the Superscript II (Invitrogen) protocol. Real time PCR was performed with SYBR Green qPCR master mix (Applied Biosystems) in a Step One plus real-time PCR detection system (Applied Biosystems). All amplifications were performed in duplicate. Mean values of triplicate measurements were calculated according to the $-\Delta\Delta$Ct quantification method, and were normalized against the expression of the *36B4* or *28S* reference genes. Each PCR run also included non-template controls containing all reagents except cDNA, and generated no amplification. Specificity was confirmed by analyzing the melting curves of PCR products. Sequences of the oligonucleotides are listed in the Supplementary Information (Supplementary Table S1).

RNA interference

The generation of 'mock' and 'CNOT7kd' cells has already been described (22). The siRNA sequences targeting the CNOT7 isoforms are listed in the Supplementary Information (Supplementary Table S2). The siRNA sequences targeting both CNOT7 variants corresponded to the coding regions 463–480 (siCNOT7). The following siRNA duplexes were also used (Dharmacon Research): non-targeting control siRNA (D-001810-10) and CNOT8 (D-018791-01). One million cells were plated in a 10 mm culture dish and transfected with a final concentration of 25 nM of each siRNA duplex using Lipofectamine 2000 (Thermo Scientific), according to the manufacturer's instructions.

GST pull-down assay

GST fusions of BTG1, BTG2, PRMT1, CNOT7v1 and CNOT7v2 proteins were expressed in *Escherichia coli* and purified over glutathione-Sepharose beads. Binding assays were carried out as previously described (24).

Reporter assay

In tethering experiments, MCF7 cells, plated in 24-well plates, were transfected with 50 ng of pCI-RL-BoxB and 10 ng of pCI-FL using Lipofectamine 2000. To obtain equal expression of λN-fusion constructs, 20 ng of λN-CNOT7v1 and 100 ng of λN-CNOT7v2-encoding plasmids were used for transfections. The luciferase activity was determined using a dual luciferase assay kit (Promega) with a Luminoskan Ascent luminometer (Thermo Scientific). For the *CD44v5* splicing reporter assays, cells were co-transfected with pCI-V5-CNOT7v1/2 or pCI vectors, the *CD44v5*-Luc minigene and a control *Renilla* Luciferase-encoding plasmid. *CD44v5*-Luc minigene was also transfected in mock, siCTL and siCNOT7v1 or v2 transfected MCF7 cells. Luciferase activity was measured 24 h after transfection. Experiments with *CD44v8* minigene construct were performed in MCF7 cells, as described in (33).

In vitro deadenylation assay

The *in vitro* deadenylation assay has been described previously (10), but included the following modifications. We used synthetic biotinylated RNAs: RNA7A: 5′-UCUAAAU(A)$_7$-3′ and RNA10C: 5′-UCUAAAU(C)$_{10}$-3′, which contained 7 A and 10 C residues on their 3′ end, respectively. Degradation reactions were performed with 150 fmol of synthetic RNA in a buffer containing 10 mM Tris–HCl pH 8.0, 1 mM MgOAc, 2 mM DTT, 0.02% NP40, 2 mM spermidine. Assay reactions were initiated by adding 10 pmol of recombinant proteins and incubated at 30°C for the indicated times. After the addition of a loading buffer containing formamide, reaction products were analyzed on 15% acrylamide urea gel, electroblotted onto a positively charged nylon membrane (Amersham) and detected by streptavidin-mediated chemiluminescence using the Chemiluminescent Nucleic Acid Detection Module (Pierce), following the manufacturer's instructions.

In vitro methylation assay

The *in vitro* methylation protocol has been described previously (26). Briefly, GST-PRMT1 was incubated with GST-tagged SAM68P3 with increasing amounts of GST-CNOT7 proteins in the presence of S-adenosyl-L[*methyl*-^{3}H]methionine ([^{3}H]SAM 85 Ci/mmol) for 90 min at 37°C. Methylation reactions were quenched by the addition of an equal volume of 2 × Laemmli sample buffer, heated at 100°C for 5 min, and separated by SDS-PAGE. Following electrophoresis, gels were soaked in Amplify Fluorographic Reagent (Amersham Biosciences) according to the manufacturer's instructions and visualized by fluorography.

Exon array data analysis

Affymetrix Human Exon 1.0 ST Array dataset analysis was conducted using EASANA® (GenoSplice technology), which is based on the FAST DB® annotations (34,35). Exon Array data were normalized using quantile normalization. Background corrections were made with antigenomic probes, which were selected as described previously (36–38). We focused exclusively on probes targeting exons annotated from FAST DB® transcripts in order to study well-annotated genes, the mRNA sequences of which are readily available on public databases (34,35). Poor-quality probes (e.g. probes labeled by Affymetrix as 'cross-hybridizing') and probes with a low intensity signal, compared to antigenomic background probes with the same GC content, were removed from the analysis. Only probes with a DABG *P*-value ≤0.05 in at least half of the arrays were considered for statistical analyses (36–38). Moreover, only genes expressed in at least one compared condition were analyzed. We considered that genes were expressed if the DABG *P*-value was ≤0.05 for at least half of the gene probes. Statistical analyses of the splicing index from the Exon Array data were performed using the paired Student's *t*-test, as described previously (36–38). The splicing index represents the difference in gene-normalized exon intensity values between the two experimental conditions analyzed (36–38). Results were considered statistically significant for uncorrected *P*-values ≤0.05 and fold changes ≥1.4.

Measurement of cell proliferation and viability

One day after siRNA transfection, MCF7 cells were trypsinized and replated in triplicate in six-well plates (10^5 cells per well). One plate was prepared each day during the experimental time-course and cells were counted every 24 h using the Biorad TC20 cell counter. Similarly, the transfected cells were photographed 3 days after transfection. For bromodeoxyuridine (BrdU) incorporation analysis, 2×10^3 MCF7 cells/well were plated on a 96-well plate. After 16 h, BrdU was added to the cells at a final concentration of 10 μM and the cells were reincubated for 3 h. The detection method used was the Cell Proliferation colorimetric ELISA System (Roche), which was performed according to the manufacturer's instructions. In parallel, cell death was measured 3 days after siRNA transfection using the Cell Death Detection colorimetric ELISA kit (Roche), according to the manufacturer's instructions.

RESULTS

Characterization of the human CNOT7v2 isoform

By comparing available ESTs with the human *CNOT7* genomic sequence, we found that the *CNOT7* gene generates at least two alternatively spliced variants in human cells. The second mRNA isoform, *CNOT7v2* (NCBI RefSeq: NM_054026.3; protein ID: NP_473367.2), uses an alternative splice site in the last exon (ex7), which excludes the final coding exon (ex8) and includes an upstream intron. This splicing event results in a frameshift and an earlier stop codon compared to the longer isoform: *CNOT7v1* (NCBI RefSeq: NM_013354.6; protein ID: NP_037486.2). The retained sequence displays a divergent 3′ untranslated region (3′ UTR) with an alternative polyadenylation signal (Figure 1A). This splicing event leads to the expression of a shorter protein with a 41-amino-acid deletion in its C-terminal end compared to variant 1 (See alignment in Supplementary Figure S1A).

To determine the expression profiles of CNOT7 variants, we analyzed their expression levels in normal human tissues by quantitative RT-PCR, using the *28S* gene as an internal control. As shown in Figure 1B, both v1 and predicted v2 mRNAs were co-expressed in all tissues tested, with systematically higher levels of CNOT7v1. However, CNOT7v2 showed a higher degree of tissue specificity in its expression pattern and was detectable predominantly in breast tissue, and to a lesser extent, in the spinal cord (Figure 1B). The specificity of the v1 and v2 primers used for PCR quantification was validated by the transfection of siRNA duplexes in MCF7 cells. These siRNAs were designed to target the divergent 3′UTR and their efficiency was tested by RT-qPCR (Supplementary Figure S2A).

Several previous studies reported the presence of two forms of CNOT7 in human cultured cell lines, namely one with a molecular mass of 32 kDa and a slower migrating isoform at 30 kDa (26,28,39). We tested whether the v2 protein was detected by western blot in the soluble protein extracts of the mammary carcinoma cell line MCF7, using the anti-CNOT7 affinity-purified polyclonal antibody as previously described (26). As shown in Figure 1C, the anti-CNOT7 antibody detected a slower migrating band, in addition to

the 32 kDa protein, which disappeared in cells stably expressing a shRNA targeting the CNOT7 isoforms. Moreover, we performed an extraction and western blot analysis of total proteins from MCF7 cells. The anti-CNOT7 immunoblot revealed multiple slower migrating bands between 28 and 30 kDa (Figure 1D). The accumulation of two specific bands was efficiently decreased by the transfection of specific siRNA duplexes targeting CNOT7v2. We confirmed by RT-qPCR that knockdown of CNOT7v2 mRNA was achieved at mRNA level and did not affect the expression level of CNOT7v1 (Supplementary Figure S2B). Overall, these data indicate that the CNOT7v2 variant is detectable in MCF7 cells alongside the v1 protein, although at lower levels, and possibly as a post-translationally modified protein.

We next examined the sub-cellular localization of each isoform in human cells. Endogenous CNOT7 was mainly detected in the cytoplasm, as well as in nuclear speckles where it co-localizes with its partner, PRMT1, and the nuclear speckle marker SC35, as previously described (26) (Supplementary Figure S1B). Since the anti-CNOT7 antibody recognizes both isoforms, we transfected MCF7 cells with plasmids expressing V5-tagged CNOT7 isoforms and the intracellular distribution of each isoform was subsequently analyzed by immunofluorescence. Interestingly, CNOT7v2 expression predominantly resulted in a punctuated nuclear staining, while CNOT7v1 was mainly present in the cytosol (Figure 1E). The presence of CNOT7v2 in nuclear foci was also observed in a glioma U251 cell line (Supplementary Figure S1C and D). This differential localization may, therefore, result in a functional divergence of the CNOT7 isoforms in the regulation of RNA decay and nuclear processes.

CNOT7v2 does not display intrinsic deadenylase activity

The CNOT7 protein is a member of the DEDD superfamily 3′-5′ exonucleases, characterized by the presence of four acidic amino-acids: three aspartates (D) and one glutamate (E). These residues are involved in catalysis through the coordination of two Mg^{2+} ions (sites A and B) in the active site. In order to explore whether the absence of the CNOT7v1-specific region influences CNOT7v2 function, a homology model of CNOT7v2 was constructed using the SWISS-MODEL server (40) (Figure 2A). CNOT7v1 (PDB ID: 4GMJ) was used as the template of the homology model. The validation analysis (Ramachandran plot) of the CNOT7v2 model indicated that 97.9% of amino acid residues are located in favoured regions (Supplementary Figure S3A). Structural superimposition revealed that modelled CNOT7v2 does not exhibit any structural difference as compared to CNOT7v1 (Figure 2A). Moreover, the enlarged view of the catalytic site showed that CNOT7v2 is likely to adopt the core catalytic domain of the RNase D superfamily, characterized by the DEDD sequence motif (Figure 2A).

We next tested whether human CNOT7v2 is actively involved in mRNA degradation *in vitro*, as we previously reported for the v1 protein (10). Recombinant proteins of both isoforms were incubated with a 5′ end biotin-labelled synthetic RNA oligonucleotide (RNA7A) with 7 A residues
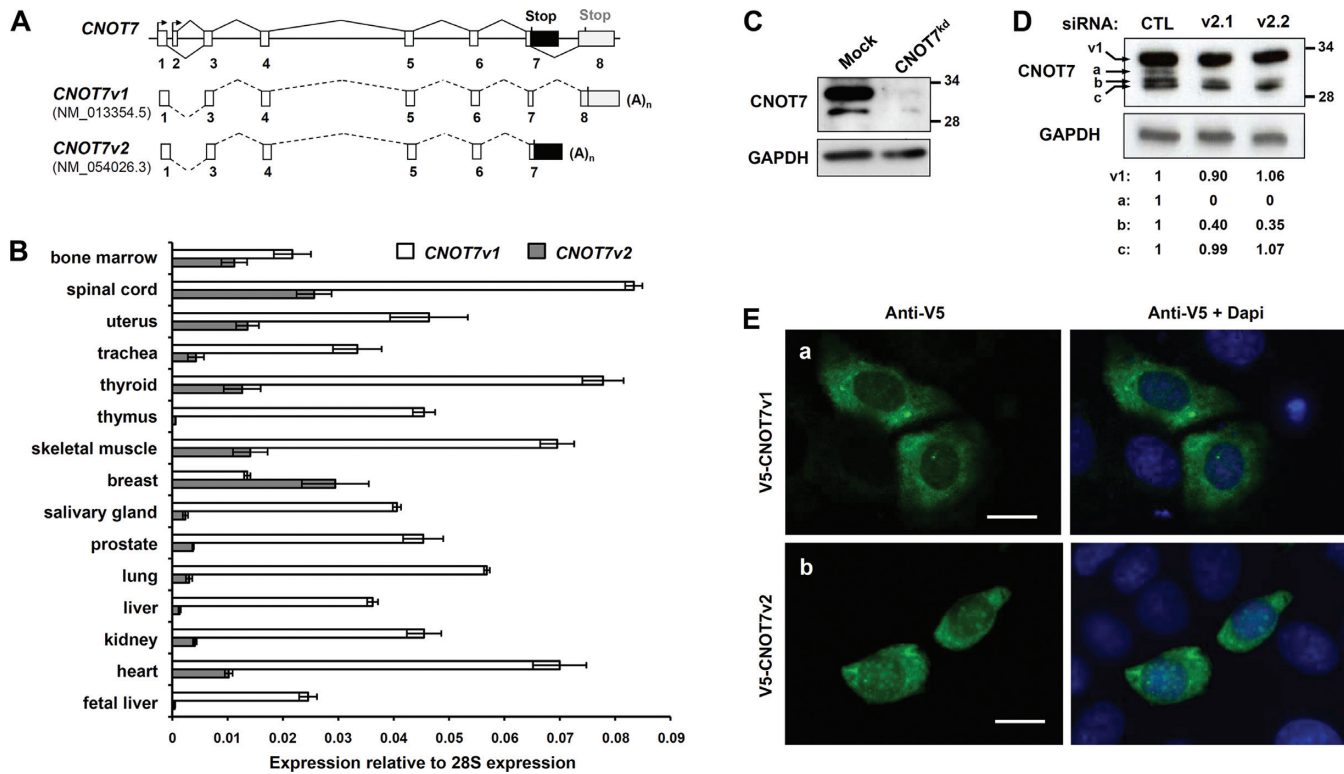
Figure 1. Genomic organization and characterization of *CNOT7* isoforms. (**A**) Schematic representation of the *CNOT7* gene leading to the formation of the two *CNOT7* isoforms, *CNOT7v1* and *CNOT7v2*, through an alternative splicing. Exons are shown as boxes. The *CNOT7* variant 2 uses alternate splice sites in its last exon, resulting in a frameshift and an earlier stop codon compared to variant 1. The encoded CNOT7v2 is shorter and has a distinct C-terminal. (**B**) Expression of *CNOT7* isoforms in human tissues. Total RNA isolated from human tissues was reverse transcribed and cDNA were amplified by qPCR using isoform-specific oligonucleotides. Gene expression levels were normalized against the internal *28S* control. All of the qPCR experiments were performed in triplicate and are expressed as mean values ± standard deviations (SD) of three independent experiments. (**C**) MCF7 cells were stably transfected with vectors expressing control shRNA (mock) or shRNA targeting *CNOT7* transcripts (CNOT7^{kd}). Soluble proteins were prepared to test CNOT7 expression. (**D**) Total extracts (20 μg) from MCF7 cells transfected with non-targeting control (CTL) or two specific CNOT7v2 siRNA duplexes (v2.1 and v2.2) were analyzed by western blot with the indicated antibodies. Western blot bands were quantified by ImageJ, normalized against GAPDH and compared to CTL extracts. The numbers below the bands correspond to the fold change compared to the CTL extract. The efficiency of the CNOT7v2 knockdown was verified by qPCR (see Supplementary Figure S2B). (**E**) Sub-cellular localization of CNOT7 proteins in MCF7 cells. MCF7 cells were transiently transfected with N-terminal V5-tagged CNOT7 encoding pCI-Neo vectors for 24 h. Anti-V5 IF was performed following the expression of V5-tagged CNOT7v1 (a) or v2 (b). Cells were fixed in cold methanol, anti-V5 antibody was used for IF and nuclei were stained with DAPI. Cells were mounted on glass slides and the microscopic analyses were directly performed. Scale bar = 40 μm.

in its 3′ end (Figure 2B and C). The time-course analysis of the reaction products on urea-polyacrylamide gels confirmed that recombinant CNOT7v1 was able to degrade the RNA substrate, since shorter products appeared over time. Conversely, recombinant CNOT7v2 was unable to degrade the synthetic RNA (Figure 2B). We also used a 5′ biotin-labelled RNA oligonucleotide ending with 10 C residues in its 3′ end (RNA10C) as a control. This molecule was completely stable in the presence of CNOT7v1, confirming its strong specificity toward A residues and its inability to act endonucleolytically (Supplementary Figure S4A). Altogether, these data indicate that the last 41 C-terminal residues present in CNOT7v1, and absent in CNOT7v2, are crucial for conducting deadenylation, at least *in vitro*.

To rule out the possibility that the v2 protein is active in a cellular context, we tested its ability to regulate the accumulation of *IFI27*, an mRNA that we identified as a target of CNOT7 (22). We analyzed whether CNOT7v2 was involved in the regulation of *IFI27* stability by transiently knocking down its expression in MCF7 cells. The quantification of

the *IFI27* mRNA level indicated that v2 depletion does not increase *IFI27* abundancy, as opposed to CNOT7v1 (Supplementary Figure S4B). We also analyzed the decay rate of Cyclin G2 mRNA, a transcript which has been identified as destabilized by both CNOT7v1 and CNOT8 deadenylases (41). To test whether CNOT7v2 regulates the stability of this transcript, we knocked down both CNOT7 isoforms and CNOT8, by siRNA transfection. After siRNA transfection, cells were treated with actinomycin D, and total RNA was isolated at several time points. As expected, the mRNA of Cyclin G2 was stabilized after actinomycin D treatment in CNOT7v1/CNOT8 double knockdown cells. Nevertheless, no significant increase in Cyclin G2 mRNA half-life was observed in CNOT7v2 single or CNOT7v2/CNOT8 double knockdown MCF7 cells, suggesting that CNOT7v2 does not participate in the destabilization of this transcript (Supplementary Figure S4C).

We then developed a tethering assay to investigate the activity of CNOT7v2 *in cellulo*. A *Renilla* luciferase reporter mRNA containing five BoxB sequences in the 3′ UTR was
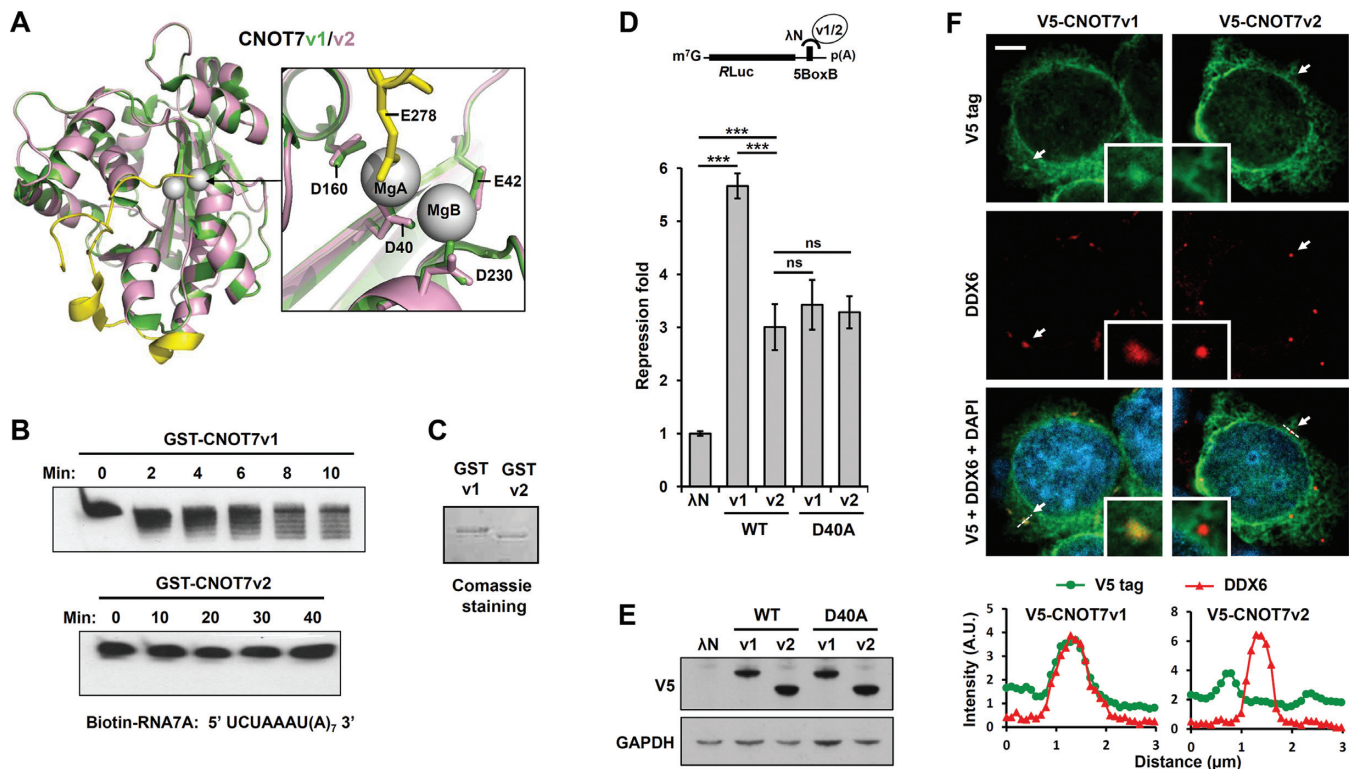
Figure 2. Activity of CNOT7 isoforms in post-transcriptional mRNA silencing. (**A**) Superposition of the homology model of CNOT7v2 (pink) and crystal structure of CNOT7v1 (green). The putative structure of CNOT7v2 was provided by the homology-modelling server Swiss-Model, using the structure of CNOT7v1 (PDB: 4GMJ) as a template. The CNOT7v1-specific C-terminal region is highlighted in yellow. The Mg^{2+} ions are shown as grey spheres. Ribbon representations were developed using PyMOL. The insert shows an enlarged view and structural comparison of their respective catalytic site. The CNOT7v1-specific residue E278 is highlighted in yellow. The model indicates the position of the Mg^{2+} ions and the side chains of amino acids D40, E42, D160, D230 and E278 which are involved for the coordination of Mg^{2+} ions. (**B**) CNOT7v2 does not display a deadenylase activity *in vitro*. A 5′ end-labelled synthetic RNA oligonucleotide ending with seven A residues was incubated with 10 pmol of the recombinant proteins at 30°C for the indicated times. The products of RNA degradation were visualized on urea-polyacrylamide gels, electroblotted onto a membrane and detected by streptavidin-mediated chemiluminescence. (**C**) SDS-PAGE and Coomassie staining of recombinant GST-CNOT7v1 and v2 proteins (5 μg per lane) used in (B). (**D**) Artificial tethering of CNOT7 isoforms to the 3′ UTR of a reporter mRNA. The upper panel shows a schematic representation of the tethering assay with the *Rluc-5boxB* reporter construct. Recruitment of CNOT7 proteins to the *Renilla* Luciferase (*R*luc) mRNA was mediated by the fused λN peptide, which has a high affinity for the BoxB sequence. Determination of luciferase activity was analyzed 24 h after transfection. *R*luc luminescence was normalized against Firefly luciferase level, and repression fold was calculated by dividing the relative luciferase activity of the cells transfected with the empty pCI-λN vector by the luciferase activity of λN-CNOT7 proteins expressing cells. The mean values (±SD) from three independent experiments are shown and the *P*-value was determined by two-tailed Student's *t*-test: (ns) non-significant, (*) $P < 0.05$; (**) $P < 0.01$; (***) $P < 0.001$. (**E**) Extracts from the MCF7 cells used in (C) were analyzed by western blot with the indicated antibodies. (**F**) Confocal images of MCF7 cells transfected with V5-CNOT7v1 or v2 and immunostained for the V5 tag (green) and DDX6 (red). Nuclei were stained with DAPI (blue). Insets show a higher magnification of a P-body (arrow). Dashed white lines in composite images identify line scans measured to determine the distribution of both DDX6 and V5-CNOT7 signals. Line plot graphs (bottom) show integrated intensity values for each panel. Intensity line scans along others DDX6 foci are presented in Supplementary Figure S5. Scale bar = 5μm.

expressed in combination with plasmids expressing CNOT7 isoforms fused to a λN peptide, which has a high affinity for the BoxB sequences (Figure 2D and E). The silencing capacity of CNOT7 variants was assessed following the measurement of luciferase activity. As expected, we observed that recruitment of λN-CNOT7v1 to the 3′ UTR markedly reduced luciferase reporter activity. Interestingly, a repression in reporter activity was also observed upon expression of λN-CNOT7v2 (3-fold repression), but to a significantly weaker extent compared to λN-CNOT7v1 (5.8-fold). The λN-CNOT7v2-dependent repression appears comparable to that of a catalytically inactive version of CNOT7v1 (λN-CNOT7v1^{D40A}), as well as the reciprocal mutant of CNOT7v2 (λN-CNOT7v2^{D40A}) (Figure 2D). These data indicate that λN-CNOT7v2 behaves similar to a catalytically inactive CNOT7 mutant vis-à-vis its silencing capacity.

As CNOT7v1 has been observed to co-localize with mammalian P-bodies, which are specific cytoplasmic foci enriched in proteins involved in mRNA metabolism (18,42), we then tested whether CNOT7v2 can also be found in P-bodies by examining subcellular localization of V5-tagged CNOT7 variants in MCF7 cells. DDX6, a well-characterized component of P-bodies, was used as a marker to visualize P-bodies by immunofluorescence microscopy (43). Although CNOT7v1 was observed to co-localize with DDX6, CNOT7v2 did not form foci that co-localized with P-bodies. Intensity line scans were performed along the DDX6 foci to confirm the absence of relationship between the spatial distribution of CNOT7v2 and P-bodies.

(Figure 2F and Supplementary Figure S5). Furthermore, CNOT7v2 knockdown cells did not show a reduced amount of P-bodies (Supplementary Figure S4D). This suggests that deadenylation is not impaired in the absence of CNOT7v2.

CNOT7v2 interacts differentially with CCR4–NOT-associated proteins

The above-mentioned data support the hypothesis of a functional divergence between the two CNOT7 isoforms, which prompted us to verify the presence of CNOT7v2 in the CCR4–NOT complex. The conserved core of the CCR4–NOT complex consists of a catalytic module containing CNOT7 and CNOT6, surrounding by CNOT9, the CNOT2/3 and CNOT10/11 modules. In addition, CNOT1 bridges the interaction between these modules and therefore acts as a scaffold protein for the assembly of the complex (44,45). As shown in Supplementary Figure S1A, CNOT7v2 conserves the residues and regions interacting with both CNOT1 and CNOT6. To shed light on the presence of CNOT7v2 in the CCR4–NOT complex, we compared the modeled CNOT7v2 structure with existing structures of conserved CCR4–NOT components containing CNOT7v1. A model was generated by superimposing the modeled CNOT7v2 structure with the MIF4G domain of human CNOT1 in complex with CNOT7v1 (PDB 4GMJ) (44). The resulting model was then superimposed with the structure of yeast Ccr4 by using the structure of the yeast Not1–Caf1–Ccr4 complex (PDB 4B8C) (45). Structural alignments and molecular graphics confirmed that CNOT7v2 displays the interaction surfaces which are necessary for its incorporation into CCR4–NOT (Supplementary Figure S3B). We then examined whether this interaction occurred with endogenous CCR4–NOT by co-immunoprecipitation experiments (co-IP). Lysates from MCF7 cells transfected with vector expressing V5-tagged CNOT7v2 (or empty vector) were subjected to anti-V5 IP, followed by immunoblotting with anti-CNOT 1, 2, 3, 6 and 10 antibodies. Interaction between V5-CNOT7v2 and other CNOT proteins were detected, indicating that CNOT7v2 integrates the CCR4–NOT complex (Figure 3A).

In order to verify whether CCR4–NOT incorporates CNOT7v2 with an occurrence similar to that of CNOT7v1, transfections of MCF7 cells were carried out using either a vector expressing V5-tagged CNOT7v1 or v2. Lysates of transfectants were subjected to anti-CNOT1 IP, followed by immunoblotting with an anti-V5 antibody (Figure 3B). We observed that both V5-CNOT7 v1 and v2 co-IP with endogenous CNOT1 at a similar level. GST pull-down assays were performed to investigate whether human CNOT6 interacted with recombinant CNOT7v2. As shown in Figure 3C, a specific retention of *in vitro*-translated CNOT6 was observed with GST-CNOT7v2, although with a lower affinity than that observed for GST-CNOT7v1. Altogether, these experiments confirm that CNOT7v2 is a subunit of CCR4–NOT.

Mammalian CNOT7 is a crucial partner of the BTG/Tob family of anti-proliferative proteins (24,31). Several members of this family have been described as adaptor proteins that mediate the recruitment of CCR4–NOT to mRNAs

(46–48). We examined an interaction between CNOT7v2 and the BTG proteins using the mammalian two-hybrid system in HEK293T cells, as previously described (24). As shown in Figure 3D, both GAL4-BTG1 and 2 significantly induced the luciferase reporter activity, when co-expressed with VP16-CNOT7v1, but not with VP16-CNOT7v2. We validated this observation using a GST pull-down assay between GST-CNOT7 variants and *in vitro*-translated Flag-BTG1 or BTG2 (Supplementary Figure S6A and B). We also generated a model in which the modelled CNOT7v2, aligned with CNOT7v1 (PDB 4GMJ), was superimposed with the Tob-CNOT7 structure (PDB 2D5R). Human BTG2 (7-128) structure (PDB 3DJU) was also superimposed with the Tob (24–139) structure (Supplementary Figure S3C). Our model confirmed that CNOT7v2 does not include the region contacting the BTG/Tob domain, therefore suggesting that a CNOT7v2-containing CCR4–NOT complex is not recruited to mRNAs in a BTG/Tob-dependent manner.

Regulation of PRMT1 activity by CNOT7 proteins

Previous results from our lab and others have shown that three different forms of CCR4–NOT can be found *in vivo* with estimated sizes of 2 MDa, 1 MDa and 650 kDa (28,49). Therefore, we performed size exclusion chromatography using whole lysates from MCF7 cells to characterize the fractionation profile of CNOT7v2. Cellular extracts were fractionated using a Superose 6 column, and subjected to immunoblot analysis. As previously published, CNOT7v1 is detected as three distinct complexes with the expected molecular masses (Figure 4A). Remarkably, CNOT7v2 is restricted to the 2 MDa CCR4–NOT complexes. Both CNOT7 variants may co-exist in these fractions at similar levels, as suggested by the equivalent intensity of their respective bands (Figure 4A, see fractions 4, 5 and 6). We also analyzed the fractionation profile of PRMT1, a methyltransferase enzyme, which is functionally and physically associated with CNOT7 (26). We found that PRMT1 co-fractionated with the CNOT7 variants exclusively at the level of the 2 MDa complexes (Figure 4A). Therefore, we next investigated whether PRMT1 interacts with CNOT7v2 by using a GST pull-down assay. As shown in Figure 4B, a specific retention of CNOT7v2 with GST-PRMT1 was observed. An interaction was also detected with *in vitro* translated CNOT7v1 but to a lesser extent to that of CNOT7v2. The preferential association of PRMT1 with the shorter v2 protein was tested by a mammalian two-hybrid assay using the VP16-CNOT7v1/v2 and GAL4-PRMT1-expressing vectors (Figure 4C). We confirmed that PRMT1 displays a stronger affinity for CNOT7v2 than the v1 isoform. We previously demonstrated that CNOT7 regulates the PRMT1-dependent methylation of SAM68 (26). Therefore, we tested whether CNOT7v2 could affect the ability of PRMT1 to methylate SAM68. An *in vitro* methylation assay was performed in the presence of S-adenosyl-[*methyl*-^{3}H]-L-methionine as a methyl donor, using recombinant GST-PRMT1, which is enzymatically active when incubated with the fragment P3 of SAM68 fused to GST (GST-SAM68P3). SAM68P3 is a 24 amino acid peptide which contains multiple RGG repeats, and was used herein as substrate to eval-
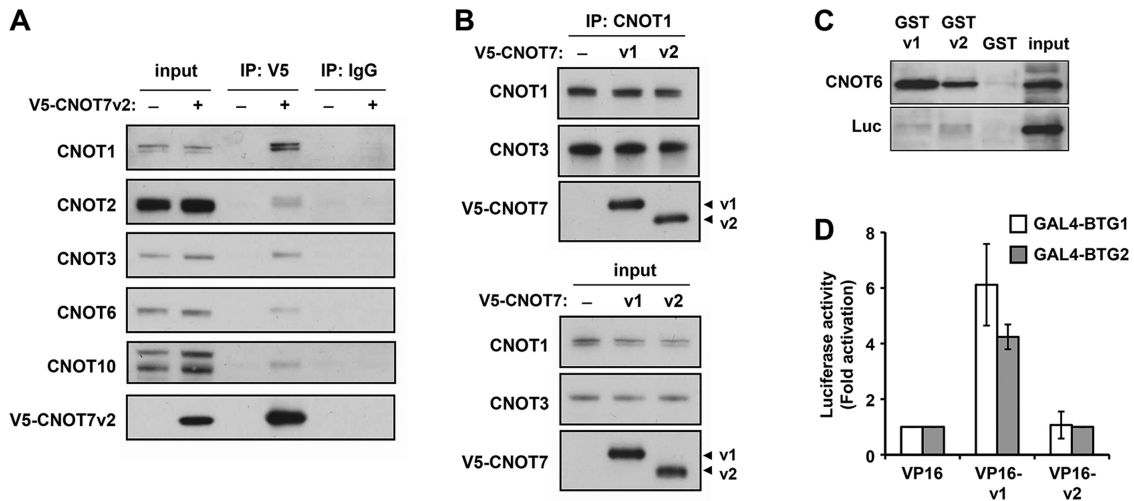
Figure 3. CNOT7v2 is a CCR4–NOT subunit. (**A**) Interaction of CNOT7v2 with CCR4–NOT components. Vector expressing V5-CNOT7v2 (or control plasmid) was transfected into MCF7 cells. Lysates of transfectants were immunoprecipitated (IP) with either normal mouse IgG or anti-V5 antibody. Total lysates (input) and eluted fractions were analyzed on a 4–12% SDS-PAGE gel, followed by immunoblotting with the indicated antibodies. (**B**) Interaction of CNOT7 isoforms with endogenous CNOT1. Vectors expressing V5-CNOT7v1 or v2 (or control plasmid) were transfected into MCF7 cells. Extracts were immunoprecipitated with anti-CNOT1 antibody. Total lysates (input) and eluted fractions were analyzed with the indicated antibodies. (**C**) Interaction between CNOT7v2 and CNOT6 was analyzed by GST pull-down experiments. *In vitro* translated biotin-labelled CNOT6 was incubated with an equivalent amount of GST, GST-CNOT7v1 or GST-CNOT7v2 bound to glutathione-Sepharose beads. The input (10%) and eluted proteins were analyzed by SDS-PAGE, electroblotted on a membrane and detected by streptavidin-mediated chemiluminescence. Biotin-labelled luciferase was tested in parallel as a negative control. GST fusion proteins used in this assay were shown by Coomassie blue staining (Supplementary Figure S6A). (**D**) A mammalian two-hybrid assay was used to analyze the interaction of CNOT7 variants with BTG proteins. Coding sequences of BTG1 and 2 were inserted in frame with the GAL4 binding domain, and CNOT7v1/v2 coding sequences with the VP16 transactivation domain. The pG4-TK-Luc reporter plasmid contains 6 GAL4 binding elements, upstream of the thymidine kinase minimal promoter region fused to the luciferase reporter gene. The interaction between the GAL4 and VP16 fusion proteins results in an increase in luciferase expression. Luciferase activities were measured in MCF7 cells 24 h post transfection and are expressed as the fold increase over the luciferase activity of the reporter vector alone.

uate the abilities of purified CNOT7 isoforms to regulate PRMT1 activity. Figure 4D shows that CNOT7v2 strongly inhibited the activity of PRMT1 compared to CNOT7v1. Increasing amounts of control GST had no effect on the methylation of SAM68P3. While this assay is valuable to reveal the ability of CNOT7v2 to modulate PRMT1 function, it does not obviously recapitulate the physiological conditions of PRMT1-dependent SAM68 methylation because the optimal PRMT1 activity depends on the substrate sequence context and its association with others cofactors (50). Indeed only a short fragment (P3) of SAM68 was used as *in vitro* substrate, while full-length SAM68 contains multiple RGG boxes and RG-rich repeats neighboring P3, which are methylated *in vivo* (51). To further analyze the relationship between PRMT1 and CNOT7 variants in the context of intact cells, we overexpressed either Flag-CNOT7v1 or v2 in MCF7 cells and performed immunoprecipitation experiments on cell lysates using an anti-SAM68 antibody. Immunoblotting was performed by using ASYM24 antibody which recognizes asymmetric dimethyl-arginine-glycine repeats. As shown in Figure 4E, the expression of CNOT7v2, and v1 to a lesser extent, increased the ability of SAM68 to be recognized by ASYM24, further suggesting that CNOT7 variants stimulate the methylation of SAM68 *in vivo*. The resulting western blot analysis confirmed that similar amounts of protein IP under each condition. We then immunoblotted these SAM68 IP with anti-PRMT1 and anti-Flag antibodies. Results showed that the overexpression of Flag-CNOT7v2 increased the as-

sociation between endogenous PRMT1 and SAM68. We also detected a preferential interaction between SAM68 and CNOT7v2 (Figure 4F). Together with our *in vitro* experiments, these results demonstrate that CNOT7v2 associates with SAM68 and regulates its methylation, possibly by increasing the recruitment of PRMT1. SAM68 exhibits a nucleoplasmic distribution but is also concentrated within distinct structures called SAM68 nuclear bodies (52). To confirm the association between CNOT7v2 and SAM68, we performed a double staining of V5-tagged CNOT7v2 and SAM68 in MCF7 cells. Confocal microscopy revealed that the sub-nuclear pattern of CNOT7v2 appears to partially co-localize with some SAM68 containing foci (Figure 4G). We performed an intensity line scan along a CNOT7v2 enrichment domain in the nucleus. This scan confirmed that CNOT7v2 overlapped at least partially with the spatial distribution of SAM68 (Figure 4H).

Several studies have shown that the PRMT1-dependent arginine methylation of SAM68 is a prerequisite for its exclusive nuclear localization and influences its RNA binding activity (51,53). To determine whether CNOT7-regulated methylation modulates the localization of SAM68, MCF7 cells were transfected with siRNAs specifically targeting CNOTv1, CNOT7v2 or both, as described above. The localization of SAM68 in these cells was detected by indirect immunofluorescence (Supplementary Figure S7A). Although we observed that SAM68 is mainly detected in the nucleoplasm in control cells, depletion of both CNOT7 isoforms resulted in the accumulation of the SAM68 protein in
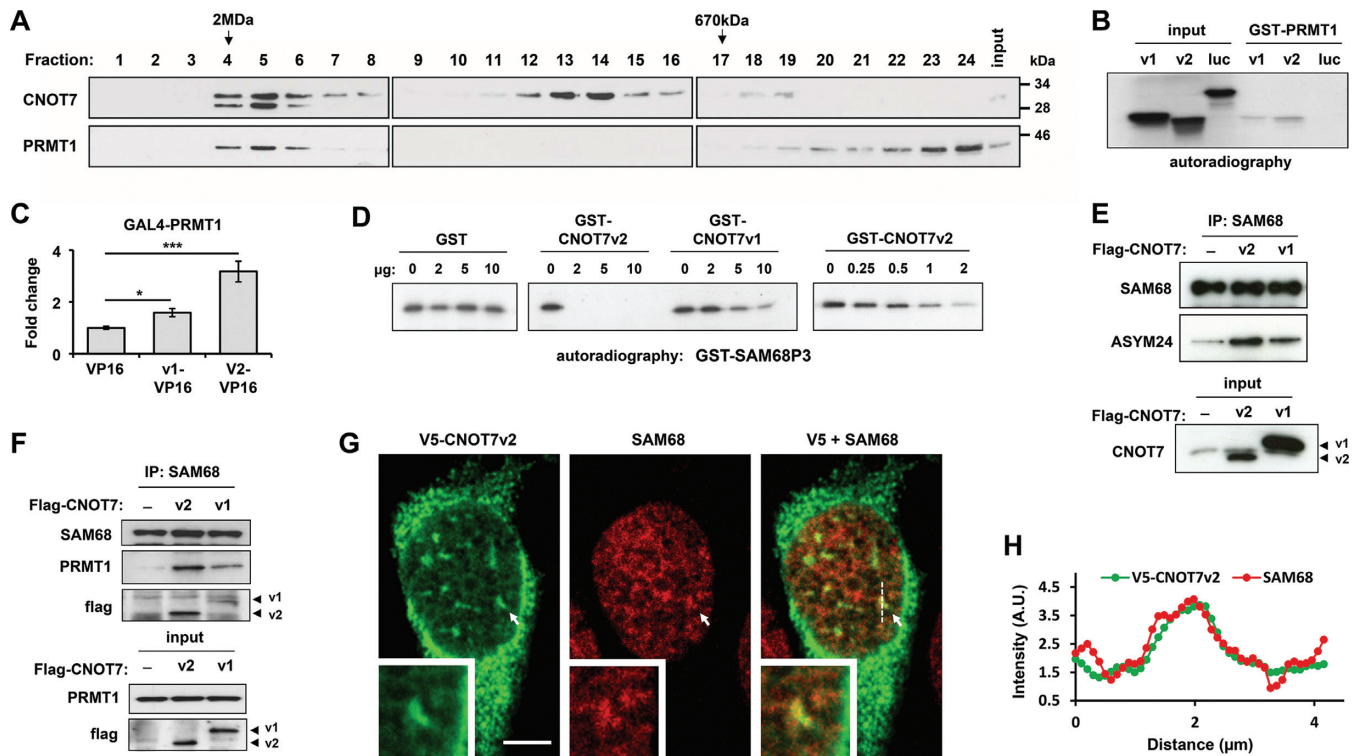
Figure 4. CNOT7v2 interacts with PRMT1 and regulates SAM68 methylation. (**A**) MCF7 cell lysate was analyzed by gel filtration chromatography using a Superose 6 (HR10/30) column. Collected fractions and input extracts (15 μg) were analyzed by SDS-PAGE. Western blots were performed using anti-CNOT7 and anti-PRMT1 antibodies. (**B**) Interaction between CNOT7v2 and PRMT1 was analyzed by GST pull-down experiments. ^{35}S-labelled *in vitro* translated CNOT7v1, CNOT7v2 and luciferase were incubated with GST-PRMT1 bound to glutathione-Sepharose beads. The eluted proteins and 1/50 of input radiolabelled proteins were analyzed by SDS-PAGE and visualized by autoradiography. (**C**) Mammalian two-hybrid assay for assessing the *in vivo* interaction of PRMT1 with CNOT7 variants. The illustrated experiments were performed in triplicate, expressed as mean values of three independent experiments. Standard deviations are shown and the *P*-value was determined by two-tailed Student's *t*-test: (*) $P < 0.05$; (***) $P < 0.001$. (**D**) Effect of CNOT7 isoforms on *in vitro* PRMT1 activity. GST-PRMT1 (1 μg) was incubated with 1 μg of GST-SAM68P3 in the presence of [^{3}H]AdoMet without or with increasing amounts of GST-CNOT7v1, GST-CNOT7v2 or GST for 90 min at 37°C. The reaction mixtures were resolved on SDS-PAGE and visualized by autoradiography. (**E**) Extracts from MCF7 transfected with vectors containing CNOT7v1 or v2 (or control vector) were immunoprecipitated using anti-SAM68 antibody and analyzed by immunoblot. The membrane was incubated with ASYM24, and then reprobed with anti-SAM68 antibody after stripping. (**F**) Extracts from MCF7 cells transfected with vectors containing CNOT7v1 or v2 (or control vector) were immunoprecipitated using anti-SAM68 antibody, then analyzed by western blotting with the indicated antibodies. (**G**) Partial co-localization of V5-CNOT7v2 and endogenous SAM68. MCF7 cells were transiently transfected with a pCI vector encoding V5-CNOT7v2, and were fixed, permeabilized, co-immunostained with anti-V5 (green) and anti-SAM68 (red) antibodies and visualized by confocal microscopy. Nuclei were stained with DAPI (blue). The right boxed inset displays higher magnification images corresponding to the region indicated by the arrow. Dashed white line in composite images identify line scan measured to determine the distribution of both SAM68 and V5-CNOT7v2 in (H). Scale bar = 5 μm. (**H**) Line scan graph shows the immunofluorescence intensity along the dashed white line from (G). The panels (A), (B), (D), (E) and (F) are representative of three independent experiments.

the cytoplasm, particularly in CNOT7v2-depleted cells, and to a lesser extent in CNOT7v1-depleted cells. This effect was also visualised by intensity line scan graphs along the cells (Supplementary Figure S7B). This distribution of SAM68 in both the cytoplasm and nuclei of CNOT7-depleted cells correlates with the observation that SAM68 is more recognized by ASYM24 following CNOT7 overexpression (Figure 4E). Altogether these results indicate that CNOT7 proteins are required to maintain SAM68 in the nucleoplasm where it normally resides, most likely via the regulation of its methylation. Due to the roles of nuclear SAM68 and PRMT1-dependent methylation in mRNA processing and alternative splicing (reviewed in (54)), we next determined whether CNOT7 variants could modulate alternative splicing.

CNOT7v2 regulates alternative splicing

We previously published the list of CNOT7-regulated transcripts in MCF7 cells, identified using an Affymetrix Human Exon 1.0 ST Array (22). This array contained probes targeting >1 million exons from well-annotated or computationally-predicted genes. For each gene, the average intensity of the exonic probes was calculated in order to quantify its level of expression. These high-density microarray datasets were re-analyzed in the context of our present study, in light of the possible role of CNOT7 proteins in the modulation of alternative splicing. We focused on the splicing profiles at the level of the exons across control and CNOT7-depleted MCF7 cells, and discovered alterations in alternative splicing in CNOT7-depleted cells. Indeed, our data highlighted 35 transcripts, in which at least one exon exhibited a fold difference (≥1.4-fold) in its level of expression, as a result of CNOT7 knockdown. Notably,

as shown in the Supplementary Table S3, the CNOT7 isoforms promoted the inclusion of 21 exons and skipping of 14 exons, confirming that CNOT7 proteins have a significant impact on the splicing activity within the MCF7 transcriptome (Figure 5A). Interestingly, among the CNOT7-regulated exons, one was specific for the *CD44* gene. Its specific alternative splicing pattern, namely the inclusion of the variable exon 8, was altered by the knockdown of CNOT7 isoforms. *CD44* encodes nine variable exons shared between its constitutive exons (Figure 5B), and SAM68 has been described to play a strategic role in the alternative splicing of *CD44* (55,56). Of note, the association of CNOT7v2 and SAM68 prompted us to select *CD44* as a model system to dissect the nuclear function of CNOT7v2 in alternative splicing. Since SAM68 is known to promote the inclusion of exon v5 into *CD44* mRNA, the role of CNOT7 variants on *CD44* variable exon v5 was also examined. Quantitative RT-PCR results showed that siRNA-mediated knockdown of CNOT7v2, but not CNOT7v1, significantly reduced the level of abundance of both *CD44v5/6* and *v8/9* mRNA (Figure 5C). Importantly, we ruled out that the effect was not the consequence of a differential regulation of *CD44* mRNA stability following CNOT7 knockdown (Supplementary Figure S8). Next, to demonstrate that CNOT7v2 inhibits *CD44* exon skipping, a minigene splicing reporter construct that contains the *CD44* v8 exon and its flanking introns was transfected into CNOT7v1- or v2-depleted MCF7 cells (Figure 5D and (33)). Splicing of the v8 exon was determined using qRT-PCR with specific primer sets that amplify v8-included and -skipped products. Knockdown of CNOT7v2, and to a lesser extent CNOT7v1, resulted in a decrease in the inclusion of v8 (Figure 5D). We also used a luciferase-based splice-reporter minigene (pETv5), in which the inclusion of exon v5 into *CD44* alters the expression of luciferase (Figure 5E and (55)). We observed a significantly higher level of expression of the luciferase in the CNOT7v2-invalidated cells (Figure 5E). In parallel, the pETv5 reporter construct was co-transfected into HEK293T cells with increasing amounts of expression constructs for each CNOT7 variant, or with an empty vector. Interestingly, the forced expression of CNOT7 variants increased the basal level of the *CD44* v5 exon inclusion in a dose-dependent manner (Figure 5E). These results therefore indicate that suboptimal amounts of CNOT7v2, and to a lesser extent CNOT7v1, enhance both exon v5 and v8 inclusion.

Modulation of *CD44* splicing is known to lead to a switch in expression from the variable exon-containing CD44v isoforms to the standard isoform, CD44s, which is devoid of all *CD44* variable exons (57). In this context, we used immunoblotting to confirm that CNOT7v2 silencing decreased the expression of a high molecular weight CD44v with a molecular mass of about 250 kDa, while favoring the production of standard CD44s 75-kDa isoforms (Figure 5F and G). After stripping, a monoclonal antibody recognizing an epitope encoded by exon v5 on the variant portion of CD44 was re-probed on the same membrane. As shown in Figure 5F, this antibody reacted with a 250 kDa band which co-migrates with the high molecular weight CD44v previously described. We concluded that the depletion of CNOT7v2 reduced the accumulation of a v5-containing

CD44 variant. Thus, CNOT7v2 is necessary and sufficient to stimulate *CD44* variable exon inclusion.

Role of CNOT7 isoforms in the proliferation of mammary cancer cells

The positive functions of PRMT1 and its substrate, SAM68, in neoplastic transformation have been reported in human cancers, and a switch in *CD44* splicing is known to modulate cell proliferation and invasion (for review, see (58–60)). To determine whether the CNOT7v2 isoform altered the growth potential of cells, we monitored cell proliferation and viability of MCF7 cells harboring siRNAs targeting specific CNOT7 variants. As shown (Figure 6A), cells transfected with siRNA targeting CNOT7v2 proliferated at a reproducibly slower rate than control cells. Interestingly, this dramatic effect was more pronounced than the reduction in growth observed in CNOT7v1-depleted cells. This result was observed using two different sets of targeting siRNAs and indicates that CNOT7v2 is essential for cell proliferation. To confirm this effect, proliferation of CNOT7v2-depleted cells was also examined by BrdU incorporation. BrdU ELISA measurements revealed that the siRNAs targeting CNOT7v2 led to a decrease in BrdU incorporation in transfected cells compared to control cells (Figure 6B), suggesting that CNOT7v2 knockdown reduces the number of cells in the S phase. As expected, a similar reduction in BrdU incorporation was also observed following the knockdown of CNOT7v1. Furthermore, quantitative analyses of cell death were performed by ELISA and are shown in Figure 6C. We observed that the reduction in cell growth was accompanied by an increase in cell death in both CNOT7v1 and v2-depleted cells compared to control cells. All of these effects were readily apparent three days after siRNA transfection, as observed by phase-contrast microscopy (Figure 6D). Taken together, these results reveal a role of CNOT7v2 in the proliferation and viability of MCF7 cells. Interestingly, after knockdown of CNOT7v2, we observed a marked change in the morphology of MCF7 cells (Figure 6D). We assessed the morphological change by highlighting the microtubules using α-tubulin immunostaining (Figure 6E). The control and CNOT7v1-depleted cells, which exhibited a large, polygonal-shaped, epithelial-like morphology, formed a poorly packed monolayer at confluence. In contrast, CNOT7v2-depleted cells failed to grow in an epithelium-like monolayer. The phenotype of the cells changed to a rounded-shape, the elongated projections from the cytoplasm disappeared and the cells clumped together building grape-like aggregates with disorganized nuclei.

The crucial role of CNOT7v2 in maintaining cell growth potential and morphology, as well as its high level of expression in mammary tissue, prompted us to assess whether the balance of CNOT7 isoforms might be altered in breast cancer cells. We examined the expression level of each CNOT7 transcript in three normal breast samples and breast tumors from 12 female patients by qRT-PCR. For each cDNA sample, the relative quantity of each CNOT7 variant was normalized against the *28S* gene product. We found that the relative expression ratio of the CNOT7 isoforms varied between normal and breast cancer samples. The CNOT7v1 expression level was on average 5-fold higher in breast can-
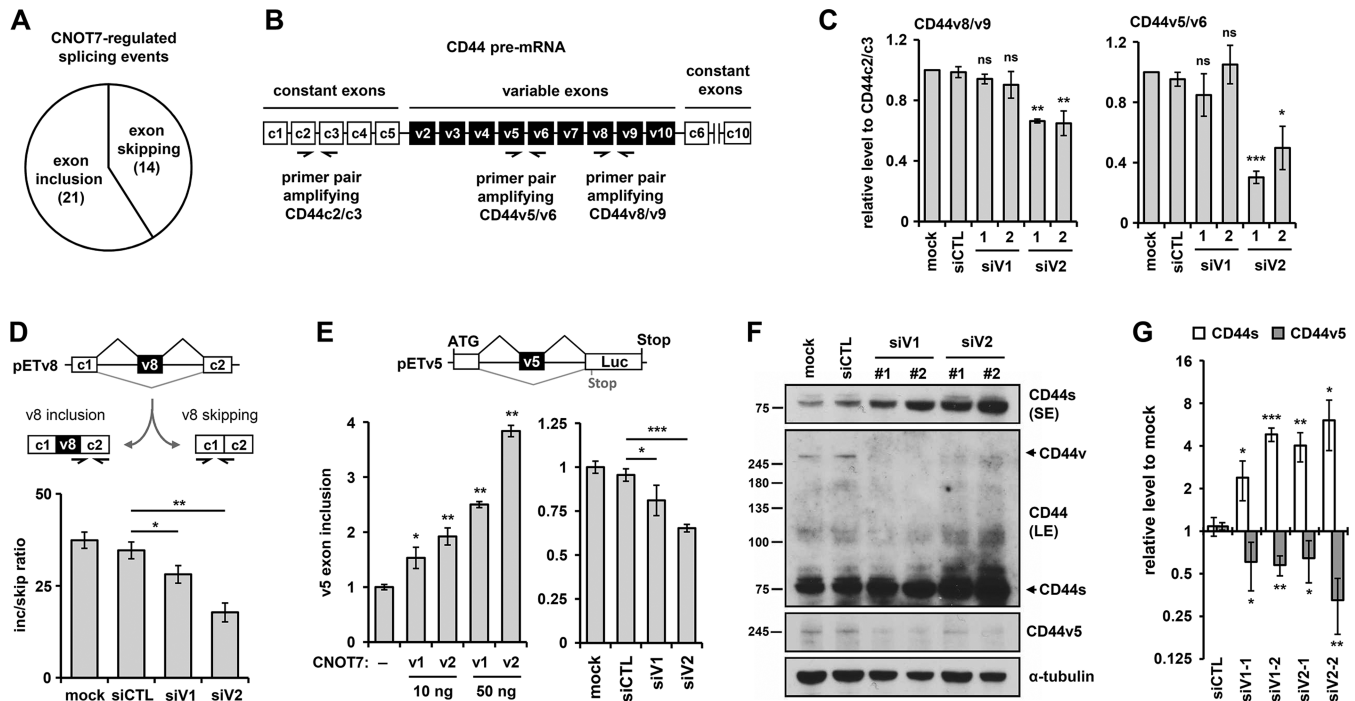
Figure 5. CNOT7v2 promotes *CD44* exon inclusion. (**A**) A pie chart showing the distribution of CNOT7-regulated cassette exon events. (**B**) Exon structure of the pre-mRNA encoding the transmembrane protein CD44, with the nine constitutive (black boxes) and nine variable exons (white boxes). Paired arrows indicate primer sets to amplify *CD44 v5/v6*, *v8/v9* and *c2/c3* containing isoforms. (**C**) qRT-PCR of *CD44* variable mRNA normalized against the constitutive *CD44c2/c3* expression level in non-transfected (mock), non-targeting control (siCTL) and CNOT7v1- or v2-knockdown MCF7 cells. Ratios of *CD44* isoforms (*CD44v5/v6*, and *CD44v8/v9*) between CNOT7 knockdown cells and control cells were plotted. (**D**,*top*) Schematic diagram of the *CD44v8* minigene construct. The v8 exon and its flanking introns are inserted between two constitutive exons as described in (33). Paired arrows indicate qPCR primer sets used to quantify both skipping and inclusion events. (*Bottom*) qRT-PCR analysis of RNA harvested from MCF7 cells transfected with the v8 minigene showing that CNOT7v2, and CNOT7v1 to a lesser extent, promotes *CD44* exon inclusion. Ratios of v8 exon inclusion and skipping were plotted. (**E**) CNOT7 proteins affect the inclusion of the *CD44* v5-exon sequence. (*Top*) A schematic representation showing the splice-reporter gene with insulin exon sequences (open boxes), *CD44* v5 exon (black box), Luciferase (Luc) coding sequence and introns (black lines); v5 exon skipping (gray) and inclusion (black) events are indicated. The lower panels show v5-luciferase splice-reporter activity of HEK293T cells co-transfected with pCI-V5-CNOT7v1/2 or pCI vectors (left panel). Two amounts of V5-tagged CNOT7 encoding pCI vectors were co-transfected in HEK293T cells with the *CD44* v5-Luc minigene and a control *Renilla* Luciferase-encoding plasmid. Firefly luciferase luminescence was normalized against *Renilla* Luciferase activity. (Right panel) *CD44* v5-Luc expression was measured in mock, siCTL and siCNOT7v1 or v2 transfected MCF7 cells. (**F**) Immunoblot analysis showing an increase in the expression of CD44 variants (CD44v) and a decrease in CD44 standard (CD44s) splice isoform level upon knockdown of CNOT7 isoforms in MCF7 cells. LE, long exposure; *SE*, short exposure. The extracts were first analysed by western blotting with an anti-CD44 antibody. The membrane was then stripped and reprobed with an anti-CD44v5. Representative of three independent experiments. (**G**) Bar graph, obtained by densitometric analysis of western blot data (F), shows quantified intensities of the CD44s and CD44v5 bands normalized against α-tubulin. The experiments illustrated in (C), (D), (E) and (G) were performed in triplicate, expressed as mean values (±SD) of three independent experiments. The *P*-value was determined by two-tailed Student's *t*-test using the 'siCTL' condition as the reference population: (ns) non-significant, (*) $P < 0.05$; (**) $P < 0.01$; (***) $P < 0.001$. The efficiency of the siRNA knockdown was verified by qPCR (see Supplementary Figure S2F and S2G).

cer samples compared to normal breast tissues (Figure 6F). Conversely, the expression pattern of v2 varied significantly among the samples. Importantly, we observed a significant overexpression of v2 transcripts in several cancer samples, suggesting that the v2 isoform can be selectively increased, relative to v1.

DISCUSSION

In the last few years, a novel model has emerged, in which the CCR4–NOT complex acts as a regulation platform, controlling gene products 'from birth to death' through the coordination of different cellular machineries. The CNOT7 subunit has been shown to play a predominant role in regulating transcription, mRNA degradation, protein turnover and signaling pathways. Here, we have reported a novel level of complexity in the function of the human CCR4–

NOT complex by characterizing a second CNOT7 isoform, which originates from the human *CNOT7* gene via alternative splicing. Altogether, our results indicate that the shorter isoform, CNOT7v2, displays distinctive functional characteristics compared to the well-characterized CNOT7v1 isoform.

Involvement of CNOT7v2 in mRNA silencing

Numerous biochemical and genetic analyses have confirmed a direct involvement of CNOT7v1 in the deadenylation process, as well as in deadenylation-independent translational control (1). Despite the conserved exonuclease domain of CNOT7v2, results from our *in vitro* assays did not reveal any deadenylase activity. This could indicate that the 41 C-terminal residues, specific to CNOT7v1, constitute a crucial region for the deadenylation function of CNOT7.
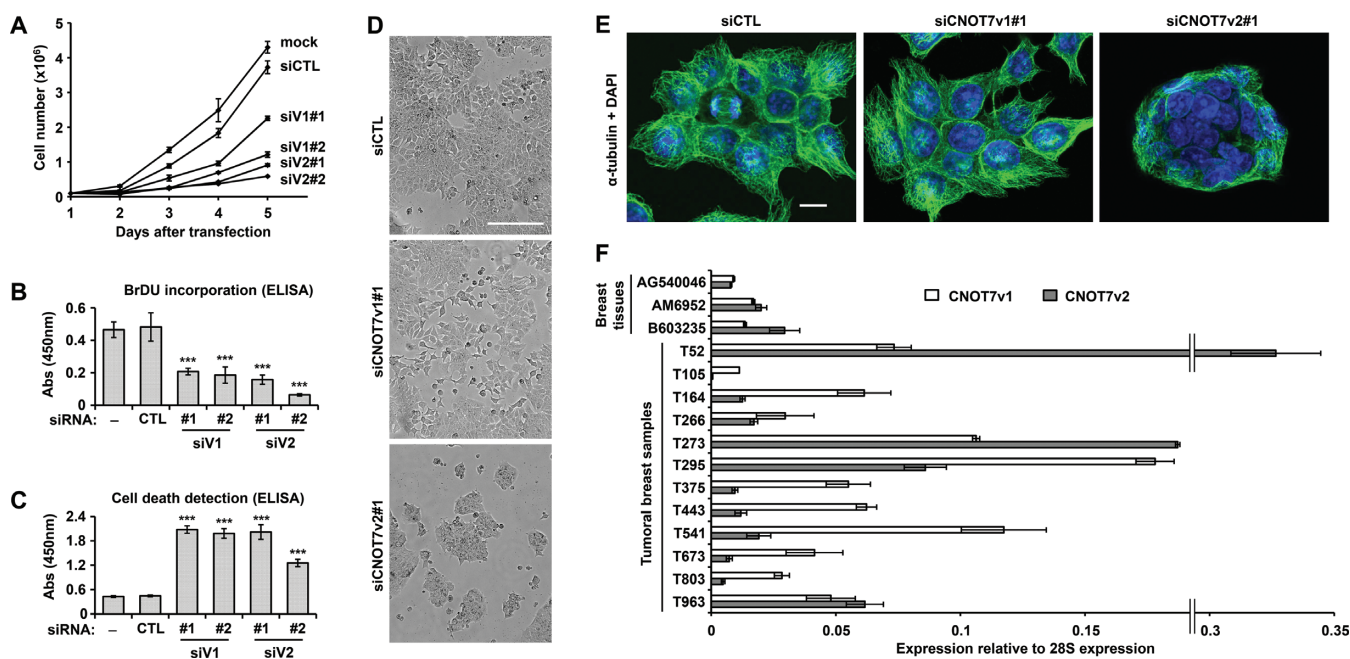
Figure 6. Phenotypes of CNOT7v1/v2-depleted MCF7 cells and expression in tumorigenic breast tissues. (**A**) Inhibition of cell proliferation by knockdown of CNOT7 isoforms. MCF7 cells were transfected with 25 nM siRNA: non-targeting control siRNA (siCTL), CNOT7v1 or CNOT7v2 targeting duplex 1 (#1) and 2 (#2), or no siRNA (mock). 10^5 cells were plated 24 h after transfection and were counted every 24 h using the Biorad TC20 cell counter. Three independent experiments were performed in triplicate. The data were expressed as averages ± SEM. (**B**) Colorimetric immunoassay for the quantification of BrdU incorporation after CNOT7v1/v2 knockdown. The cells were labelled with BrDU for 2 h at 48 h after transfection. BrDU incorporation was measured by ELISA. The experiments were performed three times in triplicate. The data were expressed as averages ± SD. (**C**) Cell death was detected using a photometric enzyme immunoassay based on the quantification of cytoplasmic histone-associated DNA fragments. The measurements were done 72 h after transfection and were performed three times in triplicate. The data were expressed as averages ± SD. (**D**) The cells were visualized three days after transfection. The experiments were performed three times and a representative image is shown. Scale bar = 200 μm. (**E**) Change in cell morphology upon CNOT7v2 knockdown. MCF7 cells transfected with non-targeting siRNA (siCTL) or against CNOT7 variants were immunostained with anti-α-tubulin (green) antibody 72 h after transfection and visualized by confocal microscopy. Nuclei were stained with DAPI (blue). Z-projects of confocal stacks are shown. Confocal microscopy is representative of at least three independent experiments. Scale bar = 10 μm. (**F**) Expression of CNOT7 variants in normal and tumorigenic breast tissues. Total RNA was extracted from normal and breast cancer tissues and expression of CNOT7 isoforms was analyzed by qRT-PCR. The normal breast sample B603235 is a pool from five different human adult donors. Gene expression levels were normalized against the internal *28S* control. All of the qPCR experiments were performed in triplicate and are expressed as mean values ± SD of three independent experiments. The P-value was determined by two-tailed Student's t-test using the 'CTL' condition as the reference population: (ns) non-significant, (*) $P < 0.05$; (**) $P < 0.01$; (***) $P < 0.001$. The efficiency of the CNOT7v1 and v2 knockdowns was verified by qPCR (see Supplementary Figure S2H).

This C-terminal CNOT7v1 region contains two residues (Glu247, Tyr260) identified by Aslam *et al.* as necessary for the interaction with BTG1/2 (41). Since the BTG proteins are known to stimulate CNOT7 deadenylase activity (61,62), this BTG-interacting region, absent in CNOT7v2, is likely to play a crucial role in maintaining the intrinsic deadenylase activity of CNOT7v1. Furthermore, Petit *et al.* raised the possibility that the C-terminal CNOT7v1 tail encompasses a glutamate (E278) which shields and coordinates the Mg^{2+} ion in the A site (Mg_A) of the catalytic pocket (44). While the relative importance of E278 vis-à-vis the function of the catalytic site of CNOT7v1 remains unknown, Petit *et al.* suggested that the C-terminal CNOT7v1 tail could be part of a mechanism for self-inhibition. Alternatively, the authors also reported that the coordination of Mg_A by E278 induces a rapprochement between the two Mg^{2+} ions which could be necessary for the hydrolysis reaction to occur, as described in the context of RNase H enzymes (44,63). Since E278 is lacking in CNOT7v2, it is tempting to speculate that the absence of the CNOT7v1-specific region could affect the geometry of the catalytic site

of CNOT7v2. Further investigation will be needed to fully resolve the structural basis of CNOT7v2 functions.

In contrast to CNOT7v1, CNOT7v2 is not present in the P-bodies and is not involved in their assembly. We also observed *in cellulo* that CNOT7v2 does not modify the expression level of natural transcripts, which have been identified as targets of CNOT7v1 activity. Altogether these data strengthen the idea that endogenous CNOT7v1 and CNOT7v2 are not redundant with regards to the control of mRNA decay. Artificial recruitment of CNOT7v2 to a reporter mRNA engenders a repression which is comparable to that of a catalytically inactive version of CNOT7v1 (D40A), indicating that CNOT7v2 does not possess an intrinsic deadenylase activity. However we noticed that both CNOTv2 and the CNOT7v1[D40A] mutant induced a significant inhibition of the reporter expression, suggesting that they may favor the recruitment of additional silencing factors, most likely the CNOT6/6L deadenylase. This point is supported by our interaction assays showing that CNOT7v2 can bind CNOT6. Therefore, CNOT7v2 shows several similarities with its Pop2p homolog in *Saccharomyces cerevisiae,* which although dispensable for catal-

ysis, contributes to the enzymatic activity of the CCR4–NOT complex by tethering Ccr4 to the Not1 scaffold (64). An additional layer of complexity in understanding the residual silencing activity of CNOT7v2 stems from the fact that CCR4–NOT can also mediate translational repression in a deadenylation-independent manner through the recruitment of various translational repressors (6,12,15,16). Therefore, it would be important to determine the relative contribution of CNOT7v2 to this specific type of silencing.

CNOT7v2, a novel subunit of the CCR4–NOT complex

Our interaction experiments indicate that CNOT7v2 is a component of CCR4–NOT, via its association with CNOT1 and CNOT6. It is plausible that both v1 and v2 proteins are competing for the same binding site on CNOT1 and CNOT6, and subsequently, the higher abundancy of CNOT7v1 in the cell can lead to a weaker integration rate of CNOT7v2 inside CCR4–NOT. Consistent with this idea, we found that endogenous CNOT7v2 is excluded from the 1 MDa and 650 kDa versions of CCR4–NOT, but is present in the 2 MDa complex. Thus CNOT7v2-containing CCR4–NOT represents a minor fraction of CCR4–NOT, indicating that only a specific subset of CCR4–NOT is available for CNOT7v2 incorporation. Moreover, our co-IP experiments suggest that CNOT1 is more enriched than the other CNOT subunits in CNOT7v2 IP (Figure 3A). Further investigations will be necessary to characterize whether the composition and integrity of CCR4–NOT is influenced by the incorporation of CNOT7v2.

The CCR4–NOT complex can be recruited to mRNAs via the interaction of CNOT7, or its CNOT8 paralog, with members of the BTG/Tob protein family (47,65,66). Both our GST pull-down and two-hybrid assays revealed an absence of physical interaction between CNOT7v2 and BTG1/2 proteins. Previous reports consolidate this observation since they identified several residues in the C-terminal region deleted in CNOT7v2, which are essential for the association with the BTG proteins (24,41,67). In this context, our data suggest the exclusion of CNOT7v2 from the BTG-dependent functional circuits involving CNOT7v1, as well as CNOT8. Recently, several labs described that the anti-proliferative activity of BTG/Tob proteins is mediated through interactions with CNOT7/8 enzymes (46,68). Therefore, it is possible that there is a dominant-negative action of CNOT7v2 on BTG-dependent anti-proliferative activity, enhanced by the competition between these deadenylases for their integration inside the CCR4–NOT complex. Further investigations are indispensable to test this hypothesis, since we have found that the relative balance of CNOT7 isoforms was altered in breast cancer samples. By contrast, Tob which has the most divergent and extended C-terminal region of the BTG/Tob family, is also capable of interacting with several residues shared between CNOT7v1 and v2 (Supplementary Figure S1A), and can concomitantly interact directly with CNOT1 via the Tob C-terminal extremity (69,70). Thus, we cannot rule out the possibility that CNOT7v2-containing CCR4–NOT maintains its ability to incorporate Tob. This speculation is of potential interest since Miyasaka *et al.* found, in a proteomic study, that Tob associates with CCR4–NOT and with dimethylarginine-containing RNA splicing/maturation factors, such as SAM68, TLS/FUS and hnRNPs (69,71).

CNOT7v2 as a regulator of arginine methylation-coupled nuclear processes

There is some ambiguity surrounding the presence of CCR4–NOT components in the nucleus and whether they are functional in regulating gene expression. In our study, we detected the presence of CNOT7v2 only in the 2 MDa CCR4–NOT complex. Interestingly, Morel *et al.* reported that this larger 2 MDa CCR4–NOT complex was the only one detectable in human cells blocked at the G0 phase, when CNOT7 localized exclusively in the nucleus (28). Altogether, these data raise the possibility that the 2 MDa CCR4–NOT complex is a nuclear version of the complex, which preferentially incorporates CNOT7v2. Moreover, our lab previously identified that human CNOT7 and the arginine methyltransferase PRMT1 interact *in vivo* and co-localize in speckles, a sub-nuclear compartment enriched in hnRNP and splicing factors (26). Here, we found that CNOT7v2 staining is predominantly restricted to nuclear foci compared to CNOT7v1, which accumulates in the cytoplasm. The sequence of both CNOT7 isoforms contains a potential basic nuclear localization motif, and CNOT7v1 has been described as a nuclear-cytoplasmic shuttling protein (39,72). Given the presence of CNOT7v2 in the nucleus and CNOT7v1 in the cytoplasm, the divergent localization of these CNOT7 isoforms is possibly due to their specific association with distinct factors. Keeping this in mind, we described a preferential affinity between CNOT7v2 and PRMT1, and a greater ability of v2 to stimulate the methylation of SAM68, a well-known PRMT1 substrate. PRMT1-dependent arginine methylation facilitates pre-mRNA splicing and affects the recruitment and nucleocytoplasmic transport of export factors (73–75). PRMT1 methylates its substrates in glycine-arginine-rich (GAR) domains, preferentially in an arginine-glycine context, which is a common feature of RNA-binding proteins (RBP). Therefore, the observations that CNOT7v2 regulates SAM68 methylation, nuclear localization and the alternative splicing of a well-known target, *CD44*, may be transposed to other GAR-containing RBP and splicing factors.

Interestingly, Timmers *et al.* examined the composition of the human CCR4–NOT complex using an in-depth proteomics approach. Analyses of associated factors revealed that most CCR4–NOT subunits co-purified nuclear RNA processing machineries, such as splicing factors and nuclear export proteins (25). Therefore, a connection between CNOT7v2 and PRMT1 is consistent with a model in which CCR4–NOT cooperates with arginine methylating enzymes in order to chaperone mRNA synthesis and maturation in the nucleus. While warranting further investigation, this view is supported by our Exon array results showing that CNOT7 proteins have an impact on the splicing activity within the transcriptome. Our findings that CD44 isoform switching is controlled by CNOT7 proteins functionally strengthen this concept. Using both *in vitro* and *in cellulo* systems, we have clearly demonstrated that CNOT7v2, and to a lesser extent CNOT7v1, regulate *CD44* alterna-

tive splicing in MCF7 cells. Nevertheless, we suspect that the contribution of CNOT7v1 is very poor, since a significant dysregulation of *CD44* splicing was only detected when CNOT7v1 overexpressed in combination with the artificial *CD44* minigenes. Several reports described the *CD44* variable exons are frequently spliced as blocks, yielding high molecular weight CD44 products (60). However, the molecular basis of this phenomenon remains to be established. Our results suggest a role for CNOT7v2 as a *trans*-factor that positively orchestrates the inclusion of *CD44* alternate exonic blocks. This idea may be exemplified by our result showing that CNOT7v2 knockdown increases the production of the shorter CD44 variant, while a high molecular variable CD44 isoform is concomitantly decreased (Figure 5F). We also found that CNOT7v2 regulates the inclusion of both v5 and v8 variable *CD44* exons. Since SAM68 has been reported mainly in v5 inclusion, it is plausible that the effect of CNOT7v2 on v8 inclusion is mediated through its concerted action on multiple GAR-containing splicing factors.

CNOT7 proteins and cancer

A crucial conclusion from this study is that alternative splicing can lead to the expression of CNOT7 variants with different biochemical properties. Importantly, we found that the expression ratio between the v1 and v2 transcripts can vary significantly among breast tumor samples. A link between CNOT7v1 and cancer progression is already established since Faraji *et al*. demonstrated that CNOT7v1 and its deadenylase activity drives tumor cell autonomous metastatic potential (76). By contrast, CNOT7v2-dependent regulation of PRMT1 activity might be linked to a plausible involvement during tumorigenesis. PRMT1 is known to catalyze the methylation of a variety of protein substrates, many of which have been linked to the development, progression and aggressiveness of different types of cancers. For instance, the methylation of SAM68 regulates its nuclear accumulation and subsequently promotes the inclusion of the v5 variable exon in *CD44* premRNA. *CD44* encodes a cell surface molecule involved in tumorigenesis, and its alternative splicing was correlated with both tumorigenesis and metastasis (reviewed in (60)). Other reports have highlighted how dysregulation of SAM68-regulated splicing events is a key step in neoplastic transformation and tumor progression (reviewed in (54)). Herein, we demonstrate that CNOT7v2 maintains a high rate of proliferation in MCF7 cells, and that CNOT7v2 knockdown leads to a dramatic growth arrest. These data provide strong evidence that dysregulation of alternative splicing of the *CNOT7* gene could be a crucial event leading to gene expression profiles that drive tumor development. Interestingly, CNOT7v2-depleted cells also exhibited a strong morphological change, suggesting a dysregulation in cell-cell adhesion. We noticed that the list of CNOT7-regulated exon events contains, in addition to *CD44*, other genes involved in cell adhesion, such as the αv integrin-encoding gene. αv integrins are exploited in cancer to promote the invasiveness of tumor cells and to manipulate the host microenvironment independently of cell growth regulation (reviewed in (77)). The unique role of CNOT7v2 in

favoring the maturation of such transcripts is likely to explain why a drastic difference on affecting cell morphology is observed between v1 and v2 isoforms, while they both behave the same in terms of regulating cell growth and viability. In future studies, it will be exciting to investigate whether a CNOT7v2-mediated splicing program is sustained to specifically modulate cell-cell adhesion to promote breast cancer metastasis.

ACCESSION NUMBER

SUPPLEMENTARY DATA

Supplementary Data are available at NAR Online.

ACKNOWLEDGEMENTS

FUNDING

REFERENCES

1. Chapat,C. and Corbo,L. (2014) Novel roles of the CCR4–NOT complex. *Wiley Interdiscip. Rev. RNA*, **5**, 883–901.
2. Collart,M.A. and Panasenko,O.O. (2012) The Ccr4–not complex. *Gene*, **492**, 42–53.
3. Wahle,E. and Winkler,G.S. (2013) RNA decay machines: deadenylation by the CCR4–NOT and Pan2-Pan3 complexes. *Biochim. Biophys. Acta*, **1829**, 561–570.
4. Goldstrohm,A.C. and Wickens,M. (2008) Multifunctional deadenylase complexes diversify mRNA control. *Nat. Rev. Mol. Cell Biol.*, **9**, 337–344.
5. Mauxion,F., Preve,B. and Seraphin,B. (2013) C2ORF29/CNOT11 and CNOT10 form a new module of the CCR4–NOT complex. *RNA Biol.*, **10**, 267–276.

6. Chen,Y., Boland,A., Kuzuoglu-Ozturk,D., Bawankar,P., Loh,B., Chang,C.T., Weichenrieder,O. and Izaurralde,E. (2014) A DDX6-CNOT1 complex and W-binding pockets in CNOT9 reveal direct links between miRNA target recognition and silencing. *Mol. Cell*, **54**, 737–750.

7. Boland,A., Chen,Y., Raisch,T., Jonas,S., Kuzuoglu-Ozturk,D., Wohlbold,L., Weichenrieder,O. and Izaurralde,E. (2013) Structure and assembly of the NOT module of the human CCR4–NOT complex. *Nat. Struct. Mol. Biol.*, **20**, 1289–1297.

8. Morita,M., Suzuki,T., Nakamura,T., Yokoyama,K., Miyasaka,T. and Yamamoto,T. (2007) Depletion of mammalian CCR4b deadenylase triggers elevation of the p27Kip1 mRNA level and impairs cell growth. *Mol. Cell. Biol.*, **27**, 4980–4990.

9. Dupressoir,A., Morel,A.P., Barbot,W., Loireau,M.P., Corbo,L. and Heidmann,T. (2001) Identification of four families of yCCR4- and Mg2+-dependent endonuclease-related proteins in higher eukaryotes, and characterization of orthologs of yCCR4 with a conserved leucine-rich repeat essential for hCAF1/hPOP2 binding. *BMC Genomics*, **2**, 9.

10. Bianchin,C., Mauxion,F., Sentis,S., Seraphin,B. and Corbo,L. (2005) Conservation of the deadenylase activity of proteins of the Caf1 family in human. *RNA*, **11**, 487–494.

11. Daugeron,M.C., Mauxion,F. and Seraphin,B. (2001) The yeast POP2 gene encodes a nuclease involved in mRNA deadenylation. *Nucleic Acids Res.*, **29**, 2448–2455.

12. Mathys,H., Basquin,J., Ozgur,S., Czarnocki-Cieciura,M., Bonneau,F., Aartse,A., Dziembowski,A., Nowotny,M., Conti,E. and Filipowicz,W. (2014) Structural and biochemical insights to the role of the CCR4–NOT complex and DDX6 ATPase in microRNA repression. *Mol. Cell*, **54**, 751–765.

13. Nishimura,T., Padamsi,Z., Fakim,H., Milette,S., Dunham,W.H., Gingras,A.C. and Fabian,M.R. (2015) The eIF4E-binding protein 4E-T is a component of the mRNA decay machinery that bridges the 5′ and 3′ termini of target mRNAs. *Cell Rep.*, **11**, 1425–1436.

14. Ozgur,S., Basquin,J., Kamenska,A., Filipowicz,W., Standart,N. and Conti,E. (2015) Structure of a human 4E-T/DDX6/CNOT1 complex reveals the different interplay of DDX6-binding proteins with the CCR4–NOT complex. *Cell Rep.*, **13**, 703–711.

15. Waghray,S., Williams,C., Coon,J.J. and Wickens,M. (2015) Xenopus CAF1 requires NOT1-mediated interaction with 4E-T to repress translation in vivo. *RNA*, **21**, 1335–1345.

16. Chapat,C., Jafarnejad,S.M., Matta-Camacho,E., Hesketh,G.G., Gelbart,I.A., Attig,J., Gkogkas,C.G., Alain,T., Stern-Ginossar,N., Fabian,M.R. *et al.* (2017) Cap-binding protein 4EHP effects translation silencing by microRNAs. *Proc. Natl. Acad. Sci. U.S.A.*, **114**, 5425–5430.

17. Eulalio,A., Behm-Ansmant,I., Schweizer,D. and Izaurralde,E. (2007) P-body formation is a consequence, not the cause, of RNA-mediated gene silencing. *Mol. Cell. Biol.*, **27**, 3970–3981.

18. Zheng,D., Ezzeddine,N., Chen,C.Y., Zhu,W., He,X. and Shyu,A.B. (2008) Deadenylation is prerequisite for P-body formation and mRNA decay in mammalian cells. *J. Cell Biol.*, **182**, 89–101.

19. Reese,J.C. (2013) The control of elongation by the yeast CCR4–NOT complex. *Biochim. Biophys. Acta*, **1829**, 127–133.

20. Badarinarayana,V., Chiang,Y.C. and Denis,C.L. (2000) Functional interaction of CCR4–NOT proteins with TATAA-binding protein (TBP) and its associated factors in yeast. *Genetics*, **155**, 1045–1054.

21. Deluen,C., James,N., Maillet,L., Molinete,M., Theiler,G., Lemaire,M., Paquet,N. and Collart,M.A. (2002) The CCR4–NOT complex and yTAF1 (yTaf(II)130p/yTaf(II)145p) show physical and functional interactions. *Mol. Cell. Biol.*, **22**, 6735–6749.

22. Chapat,C., Kolytcheff,C., Le Romancer,M., Auboeuf,D., De La Grange,P., Chettab,K., Sentis,S. and Corbo,L. (2013) hCAF1/CNOT7 regulates interferon signalling by targeting STAT1. *EMBO J.*, **32**, 688–700.

23. Winkler,G.S., Mulder,K.W., Bardwell,V.J., Kalkhoven,E. and Timmers,H.T. (2006) Human CCR4–NOT complex is a ligand-dependent repressor of nuclear receptor-mediated transcription. *EMBO J.*, **25**, 3089–3099.

24. Prevot,D., Morel,A.P., Voeltzel,T., Rostan,M.C., Rimokh,R., Magaud,J.P. and Corbo,L. (2001) Relationships of the antiproliferative proteins BTG1 and BTG2 with CAF1, the human homolog of a component of the yeast CCR4 transcriptional complex: involvement in estrogen receptor alpha signaling pathway. *J. Biol. Chem.*, **276**, 9640–9648.

25. Lau,N.C., Kolkman,A., van Schaik,F.M., Mulder,K.W., Pijnappel,W.W., Heck,A.J. and Timmers,H.T. (2009) Human CCR4–NOT complexes contain variable deadenylase subunits. *Biochem. J.*, **422**, 443–453.

26. Robin-Lespinasse,Y., Sentis,S., Kolytcheff,C., Rostan,M.C., Corbo,L. and Le Romancer,M. (2007) hCAF1, a new regulator of PRMT1-dependent arginine methylation. *J. Cell Sci.*, **120**, 638–647.

27. Kerr,S.C., Azzouz,N., Fuchs,S.M., Collart,M.A., Strahl,B.D., Corbett,A.H. and Laribee,R.N. (2011) The CCR4–NOT complex interacts with the mRNA export machinery. *PLoS One*, **6**, e18302.

28. Morel,A.P., Sentis,S., Bianchin,C., Le Romancer,M., Jonard,L., Rostan,M.C., Rimokh,R. and Corbo,L. (2003) BTG2 antiproliferative protein interacts with the human CCR4 complex existing in vivo in three cell-cycle-regulated forms. *J. Cell Sci.*, **116**, 2929–2936.

29. Elkon,R., Ugalde,A.P. and Agami,R. (2013) Alternative cleavage and polyadenylation: extent, regulation and function. *Nat. Rev. Genet.*, **14**, 496–506.

30. Di Giammartino,D.C., Nishida,K. and Manley,J.L. (2011) Mechanisms and consequences of alternative polyadenylation. *Mol. Cell*, **43**, 853–866.

31. Rouault,J.P., Prevot,D., Berthet,C., Birot,A.M., Billaud,M., Magaud,J.P. and Corbo,L. (1998) Interaction of BTG1 and p53-regulated BTG2 gene products with mCaf1, the murine homolog of a component of the yeast CCR4 transcriptional regulatory complex. *J. Biol. Chem.*, **273**, 22563–22569.

32. Garrels,J.I. (1983) Quantitative two-dimensional gel electrophoresis of proteins. *Methods Enzymol.*, **100**, 411–423.

33. Xu,Y., Gao,X.D., Lee,J.H., Huang,H., Tan,H., Ahn,J., Reinke,L.M., Peter,M.E., Feng,Y., Gius,D. *et al.* (2014) Cell type-restricted activity of hnRNPM promotes breast cancer metastasis via regulating alternative splicing. *Genes Dev.*, **28**, 1191–1203.

34. de la Grange,P, Dutertre,M, Martin,N and Auboeuf,D. (2005) FAST DB: a website resource for the study of the expression regulation of human gene products. *Nucleic Acids Res.*, **33**, 4276–4284.

35. de la Grange,P, Dutertre,M, Correa,M. and Auboeuf,D. (2007) A new advance in alternative splicing databases: from catalogue to detailed analysis of regulation of expression and function of human alternative splicing variants. *BMC Bioinformatics*, **8**, 180.

36. Wang,E., Aslanzadeh,V., Papa,F., Zhu,H., de la Grange,P. and Cambi,F. (2012) Global profiling of alternative splicing events and gene expression regulated by hnRNPH/F. *PLoS One*, **7**, e51266.

37. Gandoura,S., Weiss,E., Rautou,P.E., Fasseu,M., Gustot,T., Lemoine,F., Hurtado-Nedelec,M., Hego,C., Vadrot,N., Elkrief,L. *et al.* (2013) Gene- and exon-expression profiling reveals an extensive LPS-induced response in immune cells in patients with cirrhosis. *J. Hepatol.*, **58**, 936–948.

38. Colombrita,C., Onesto,E., Buratti,E., de la Grange,P., Gumina,V., Baralle,F.E., Silani,V. and Ratti,A. (2015) From transcriptomic to protein level changes in TDP-43 and FUS loss-of-function cell models. *Biochim. Biophys. Acta*, **1849**, 1398–1410.

39. Bogdan,J.A., Adams-Burton,C., Pedicord,D.L., Sukovich,D.A., Benfield,P.A., Corjay,M.H., Stoltenborg,J.K. and Dicker,I.B. (1998) Human carbon catabolite repressor protein (CCR4)-associative factor 1: cloning, expression and characterization of its interaction with the B-cell translocation protein BTG1. *Biochem. J.*, **336**, 471–481.

40. Biasini,M., Bienert,S., Waterhouse,A., Arnold,K., Studer,G., Schmidt,T., Kiefer,F., Gallo Cassarino,T., Bertoni,M., Bordoli,L. *et al.* (2014) SWISS-MODEL: modelling protein tertiary and quaternary structure using evolutionary information. *Nucleic Acids Res.*, **42**, W252–W258.

41. Aslam,A., Mittal,S., Koch,F., Andrau,J.C. and Winkler,G.S. (2009) The CCR4–NOT deadenylase subunits CNOT7 and CNOT8 have overlapping roles and modulate cell proliferation. *Mol. Biol. Cell*, **20**, 3840–3850.

42. Cougot,N., Babajko,S. and Seraphin,B. (2004) Cytoplasmic foci are sites of mRNA decay in human cells. *J. Cell Biol.*, **165**, 31–40.

43. Andrei,M.A., Ingelfinger,D., Heintzmann,R., Achsel,T., Rivera-Pomar,R. and Luhrmann,R. (2005) A role for eIF4E and eIF4E-transporter in targeting mRNPs to mammalian processing bodies. *RNA*, **11**, 717–727.

44. Petit,A.P., Wohlbold,L., Bawankar,P., Huntzinger,E., Schmidt,S., Izaurralde,E. and Weichenrieder,O. (2012) The structural basis for the interaction between the CAF1 nuclease and the NOT1 scaffold of the human CCR4–NOT deadenylase complex. *Nucleic Acids Res.*, **40**, 11058–11072.

45. Basquin,J., Roudko,V.V., Rode,M., Basquin,C., Seraphin,B. and Conti,E. (2012) Architecture of the nuclease module of the yeast CCR4–NOT complex: the Not1-Caf1-Ccr4 interaction. *Mol. Cell*, **48**, 207–218.

46. Ezzeddine,N., Chen,C.Y. and Shyu,A.B. (2012) Evidence providing new insights into TOB-promoted deadenylation and supporting a link between TOB's deadenylation-enhancing and antiproliferative activities. *Mol. Cell. Biol.*, **32**, 1089–1098.

47. Hosoda,N., Funakoshi,Y., Hirasawa,M., Yamagishi,R., Asano,Y., Miyagawa,R., Ogami,K., Tsujimoto,M. and Hoshino,S. (2011) Anti-proliferative protein Tob negatively regulates CPEB3 target by recruiting Caf1 deadenylase. *EMBO J.*, **30**, 1311–1323.

48. Funakoshi,Y., Doi,Y., Hosoda,N., Uchida,N., Osawa,M., Shimada,I., Tsujimoto,M., Suzuki,T., Katada,T. and Hoshino,S. (2007) Mechanism of mRNA deadenylation: evidence for a molecular interplay between translation termination factor eRF3 and mRNA deadenylases. *Genes Dev.*, **21**, 3135–3148.

49. Bai,Y., Salvadore,C., Chiang,Y.C., Collart,M.A., Liu,H.Y. and Denis,C.L. (1999) The CCR4 and CAF1 proteins of the CCR4–NOT complex are physically and functionally separated from NOT2, NOT4, and NOT5. *Mol. Cell. Biol.*, **19**, 6642–6651.

50. Lee,D.Y., Ianculescu,I., Purcell,D., Zhang,X., Cheng,X. and Stallcup,M.R. (2007) Surface-scanning mutational analysis of protein arginine methyltransferase 1: roles of specific amino acids in methyltransferase substrate specificity, oligomerization, and coactivator function. *Mol. Endocrinol.*, **21**, 1381–1393.

51. Cote,J., Boisvert,F.M., Boulanger,M.C., Bedford,M.T. and Richard,S. (2003) Sam68 RNA binding protein is an in vivo substrate for protein arginine N-methyltransferase 1. *Mol. Biol. Cell*, **14**, 274–287.

52. Chen,T., Boisvert,F.M., Bazett-Jones,D.P. and Richard,S. (1999) A role for the GSG domain in localizing Sam68 to novel nuclear structures in cancer cell lines. *Mol. Biol. Cell*, **10**, 3015–3033.

53. Rho,J., Choi,S., Jung,C.R. and Im,D.S. (2007) Arginine methylation of Sam68 and SLM proteins negatively regulates their poly(U) RNA binding activity. *Arch Biochem. Biophys.*, **466**, 49–57.

54. Frisone,P., Pradella,D., Di Matteo,A., Belloni,E., Ghigna,C. and Paronetto,M.P. (2015) SAM68: Signal Transduction and RNA Metabolism in Human Cancer. *Biomed. Res. Int.*, **2015**, 528954.

55. Matter,N., Herrlich,P. and Konig,H. (2002) Signal-dependent regulation of splicing via phosphorylation of Sam68. *Nature*, **420**, 691–695.

56. Stoss,O., Olbrich,M., Hartmann,A.M., Konig,H., Memmott,J., Andreadis,A. and Stamm,S. (2001) The STAR/GSG family protein rSLM-2 regulates the selection of alternative splice sites. *J. Biol. Chem.*, **276**, 8665–8673.

57. Ponta,H., Sherman,L. and Herrlich,P.A. (2003) CD44: from adhesion molecules to signalling regulators. *Nat. Rev. Mol. Cell. Biol.*, **4**, 33–45.

58. Bielli,P., Busa,R., Paronetto,M.P. and Sette,C. (2011) The RNA-binding protein Sam68 is a multifunctional player in human cancer. *Endocr. Relat .Cancer*, **18**, R91–R102.

59. Nicholson,T.B., Chen,T. and Richard,S. (2009) The physiological and pathophysiological role of PRMT1-mediated protein arginine methylation. *Pharmacol. Res.*, **60**, 466–474.

60. Prochazka,L., Tesarik,R. and Turanek,J. (2014) Regulation of alternative splicing of CD44 in cancer. *Cell Signal*, **26**, 2234–2239.

61. Stupfler,B., Birck,C., Seraphin,B. and Mauxion,F. (2016) BTG2 bridges PABPC1 RNA-binding domains and CAF1 deadenylase to control cell proliferation. *Nat. Commun.*, **7**, 10811.

62. Mauxion,F., Faux,C. and Seraphin,B. (2008) The BTG2 protein is a general activator of mRNA deadenylation. *EMBO J.*, **27**, 1039–1048.

63. Nowotny,M. and Yang,W. (2006) Stepwise analyses of metal ions in RNase H catalysis from substrate destabilization to product release. *EMBO J.*, **25**, 1924–1933.

64. Tucker,M., Staples,R.R., Valencia-Sanchez,M.A., Muhlrad,D. and Parker,R. (2002) Ccr4p is the catalytic subunit of a Ccr4p/Pop2p/Notp mRNA deadenylase complex in Saccharomyces cerevisiae. *EMBO J.*, **21**, 1427–1436.

65. Ezzeddine,N., Chang,T.C., Zhu,W., Yamashita,A., Chen,C.Y., Zhong,Z., Yamashita,Y., Zheng,D. and Shyu,A.B. (2007) Human TOB, an antiproliferative transcription factor, is a poly(A)-binding protein-dependent positive regulator of cytoplasmic mRNA deadenylation. *Mol. Cell. Biol.*, **27**, 7791–7801.

66. Okochi,K., Suzuki,T., Inoue,J., Matsuda,S. and Yamamoto,T. (2005) Interaction of anti-proliferative protein Tob with poly(A)-binding protein and inducible poly(A)-binding protein: implication of Tob in translational control. *Genes Cells*, **10**, 151–163.

67. Nishida,K., Horiuchi,M., Noda,N.N., Takahasi,K., Iwasaki,N., Minami,A. and Inagaki,F. (2007) Crystallization and preliminary crystallographic analysis of the Tob-hCaf1 complex. *Acta Crystallogr. Sect. F Struct. Biol. Cryst. Commun.*, **63**, 1061–1063.

68. Doidge,R., Mittal,S., Aslam,A. and Winkler,G.S. (2012) The anti-proliferative activity of BTG/TOB proteins is mediated via the Caf1a (CNOT7) and Caf1b (CNOT8) deadenylase subunits of the CCR4–NOT complex. *PLoS One*, **7**, e51331.

69. Miyasaka,T., Morita,M., Ito,K., Suzuki,T., Fukuda,H., Takeda,S., Inoue,J., Semba,K. and Yamamoto,T. (2008) Interaction of antiproliferative protein Tob with the CCR4–NOT deadenylase complex. *Cancer Sci.*, **99**, 755–761.

70. Horiuchi,M., Takeuchi,K., Noda,N., Muroya,N., Suzuki,T., Nakamura,T., Kawamura-Tsuzuku,J., Takahasi,K., Yamamoto,T. and Inagaki,F. (2009) Structural basis for the antiproliferative activity of the Tob-hCaf1 complex. *J. Biol. Chem.*, **284**, 13244–13255.

71. Rappsilber,J., Friesen,W.J., Paushkin,S., Dreyfuss,G. and Mann,M. (2003) Detection of arginine dimethylated peptides by parallel precursor ion scanning mass spectrometry in positive ion mode. *Anal. Chem.*, **75**, 3107–3114.

72. Yamashita,A., Chang,T.C., Yamashita,Y., Zhu,W., Zhong,Z., Chen,C.Y. and Shyu,A.B. (2005) Concerted action of poly(A) nucleases and decapping enzyme in mammalian mRNA turnover. *Nat. Struct. Mol. Biol.*, **12**, 1054–1063.

73. Snijders,A.P., Hautbergue,G.M., Bloom,A., Williamson,J.C., Minshull,T.C., Phillips,H.L., Mihaylov,S.R., Gjerde,D.T., Hornby,D.P., Wilson,S.A. *et al.* (2015) Arginine methylation and citrullination of splicing factor proline- and glutamine-rich (SFPQ/PSF) regulates its association with mRNA. *RNA*, **21**, 347–359.

74. Yu,M.C., Bachand,F., McBride,A.E., Komili,S., Casolari,J.M. and Silver,P.A. (2004) Arginine methyltransferase affects interactions and recruitment of mRNA processing and export factors. *Genes Dev.*, **18**, 2024–2035.

75. Yu,M.C. (2011) The Role of Protein Arginine Methylation in mRNP Dynamics. *Mol. Biol. Int.*, **2011**, 163827.

76. Faraji,F., Hu,Y., Yang,H.H., Lee,M.P., Winkler,G.S., Hafner,M. and Hunter,K.W. (2016) Post-transcriptional control of tumor cell autonomous metastatic potential by CCR4–NOT deadenylase CNOT7. *PLoS Genet.*, **12**, e1005820.

77. Weis,S.M. and Cheresh,D.A. (2011) alphaV integrins in angiogenesis and cancer. *Cold Spring Harb. Perspect. Med.*, **1**, a006478.